Physics – Uspekhi **46** (9) 915 – 935 (2003)

REVIEWS OF TOPICAL PROBLEMS PACS numbers: 61.30Cz, **68.15.+e**, 83.70.Jr, 83.80.Xz

Dynamic properties of smectic films

V P Romanov, S V Ul'yanov

DOI: 10.1070/PU2003v046n09ABEH001628

Contents

Abstract. Theoretical and experimental research into the dynamic and correlation properties of smectic liquid-crystal films is reviewed. Both freely suspended films and films fastened to a solid substrate are considered. For smectic-A films, the intensity of X-ray scattering and the temporal correlation function of scattering intensities are analyzed. For smectics with the director tilted with respect to the layers, the intensity of scattering light is discussed. To illustrate theoretical results, available experimental data are used.

1. Introduction

Liquid crystals have been a subject of interest for many years. Interest greatly increased in recent decades due to various practical applications of liquid crystals, first and foremost in systems of information transfer and representation. Liquid crystals possess a number of unusual physical properties by virtue of their intermediate position between isotropic viscous liquids and crystalline solids. On the one hand, they exhibit such properties as optical anisotropy intrinsic in solid crystals, while on the other hand they are fluid like ordinary liquids.

V P Romanov St. Petersburg State University, Physics Department
ul. Ul'yanovskaya 1, 198504 Staryĭ Petergof, Russian Federation
Tel. (7-812) 428 45 15
E-mail: v.romanov@pobox.spbu.ru
S V Ul'yanov St. Petersburg Institute of Trade and Economics
ul. Novorossiĭskaya 50, 194018 St. Petersburg, Russian Federation
E-mail: ulyanov@infos.ru

Received 25 March 2003, revised 29 May 2003
Uspekhi Fizicheskikh Nauk **173** (9) 941 – 963 (2003)
Translated by Yu V Morozov; edited by S N Gorin

Liquid crystals differ in terms of structure. Some of them are characterized by regular orientation of molecules while the positions of their centers of mass are as random as they are in fluids. This class of liquid crystals includes, first and foremost, nematic liquid crystals with uniformly ordered molecular orientations normally given by a unit vector **n** (called the director vector), and cholesteric liquid crystals in which the prevalent molecular orientation rotates about a certain axis.

Another important class is constituted by liquid crystals characterized not only by a regular orientational structure but also by an ordered position of the centers of molecular masses that make up a construction of flat layers. Such substances are called smectic liquid crystals or smectics. Depending on the direction of the preferred molecular orientation, they are divided into smectics *A*, in which the director **n** is normal to the layer plane, and smectics *C*, where the director is tilted with respect to the layers at a certain angle θ. A turn of the director in smectic *C* films while passing from one layer to another so that angle θ is conserved gives rise to smectic C^*. The centers of molecular mass in each layer of smectics *A*, *C*, and C^* are disordered as in a two-dimensional liquid.

There are also smectic liquid crystals in which the positions of the centers of molecular mass are ordered within a given layer. These include smectics *B*, *F*, *I*, etc. As a rule, the positions of the centers of mass in such smectics make up a hexagonal structure, but the orientation of the director with respect to the layers may be different. A large variety of liquid crystals makes it possible to observe many phase transitions between such structures in one and the same substance.

Smectic liquid crystals are capable of forming stable macroscopic films containing from two to thousands of layers. Such films may be either freely suspended in a rigid frame or fastened to a substrate. Investigations into the

physical properties of thin smectic films (especially freely suspended ones) are of special interest because they provide a unique opportunity to study a two-dimensional structure unavailable in any other physical system. Properties of smectic liquid crystals in a film differ substantially from those in the bulk phase. This first and foremost refers to phase transitions that can occur in successive layers at different temperatures. Such transitions lead to the formation of smectic phases unobservable in thick slabs of the same material. The smectic structure, e.g., the tilt of the director with respect to the normal to a layer in smectics C, can vary across the film thickness. Both equilibrium and dynamic properties of thin films show strong dependence on the bounding surfaces. All these effects are functions of film thickness.

Thin smectic films have been extensively studied using various methods. To begin with, X-ray scattering techniques are employed, taking advantage of the fact that the characteristic scale of the layered structure is on the same order as the X-ray wavelength. Static properties of smectic films are examined by specular and diffuse scattering techniques, while correlation X-ray spectroscopy has been recently employed to study their dynamic properties. Much attention is given to studying the thermophysical properties of smectic films, in particular in the vicinity of phase transitions. Many film studies are performed using optical methods, first and foremost ellipsometry, which allow studying the characteristics of the surface structure. Light scattering techniques also find application for this purpose. They are extensively employed to study smectic C and C^* films showing marked fluctuations of the director.

To date, a large amount of experimental material has been accumulated concerning various processes in smectic films, and a consistent theoretical description of their static and dynamic properties has been provided. The most detailed information is available for smectics A, C, and C^*. For these systems, the theoretical description is in excellent agreement with experimental results and may be used as a reliable source of film parameters. This fact has acquired great importance in recent years when liquid crystals have begun to be extensively used in manufacturing a variety of displays.

The present review is centered on the analysis of smectic films, both freely suspended in a frame and fastened to a substrate. Dynamic properties and thermal fluctuation spectra of these films are considered. A detailed discussion of X-rays and visible-light scattering in smectic films is presented. Much attention is given to the theoretical description of the dynamics of smectic layers in the framework of a discrete model, bearing in mind that systematic treatment of this issue is virtually lacking from the literature.

2. Equations of motion of smectics

Compared with nematics, smectic liquid crystals are characterized by additional ordering. Specifically, the density of center-of-mass positions in smectic films is a periodic function along a certain distinguished direction, e.g., the axis z. This means that smectics have a layered structure formed, when in equilibrium, by a set of equidistant flat layers. The structure of each layer depends on the type of a given smectic liquid crystal. In the most important and simple case of smectic A, each layer represents a two-dimensional liquid composed of molecules whose long axes are aligned perpendicularly to the layer. The structure of a deformed smectic A can be described by a variable $u(\mathbf{r})$ that represents the displacements of layers from equilibrium positions along the z axis. The free energy of distortion in smectic A must be invariant with respect to its rotation as a whole about the x and y axes and relative to the reflection in the xy plane. In the Gaussian approximation, the distortion free energy can be written in the form [1 – 3]

$$F_{\mathrm{b}} = \frac{1}{2}\int \left\{ B\left(\frac{\partial u(\mathbf{r})}{\partial z}\right)^2 + K\left[\Delta_\perp u(\mathbf{r})\right]^2 \right\} \mathrm{d}\mathbf{r}\,, \tag{2.1}$$

where $\Delta_\perp = \partial^2/\partial x^2 + \partial^2/\partial y^2$ is the Laplace operator in the xy plane, B is the elastic constant related to the compression and rarification of the layers, and K is the elastic constant related to their bending. In the free energy of smectic films, the surface contribution is as important as the bulk one [4]

$$F_{\mathrm{s}} = \frac{\gamma}{2}\int \left(\left|\nabla_\perp u_{\mathrm{s}_1}(\mathbf{r}_\perp)\right|^2 + \left|\nabla_\perp u_{\mathrm{s}_2}(\mathbf{r}_\perp)\right|^2 \right) \mathrm{d}\mathbf{r}_\perp\,, \tag{2.2}$$

where γ is the surface tension and $u_{\mathrm{s}_1}(\mathbf{r}_\perp)$ and $u_{\mathrm{s}_2}(\mathbf{r}_\perp)$ are the displacements of the two free film surfaces from the equilibrium position.

For the purpose of describing motions in smectic films, they may be regarded as incompressible, since these motions occur with velocities that are much lower than the speed of sound c, and the inequality $\omega \ll cq$ is assumed to be valid for both the circular frequency ω and the wave number q. In this case the motion in smectic A is described by the following system of equations [1 – 3]:

$$\begin{aligned} &\partial_i v_i = 0\,, \\ &\rho\,\frac{\partial v_i}{\partial t} = -\partial_i p + \partial_j \sigma'_{ij} + h\delta_{iz}\,, \quad i = x, y, z\,, \\ &\frac{\partial u}{\partial t} = v_z + \lambda_{\mathrm{p}} h\,. \end{aligned} \tag{2.3}$$

Here, v_i are the velocity components, p is the pressure, λ_{p} is the permeation constant, and h is the molecular field, the expression for which has the form

$$h = B\,\frac{\partial^2 u}{\partial z^2} - K(\Delta_\perp)^2 u\,. \tag{2.4}$$

In Eqns (2.3), summation over repeated indices is implied and the following notation is used:

$$\partial_x \equiv \frac{\partial}{\partial x}\,, \quad \partial_y \equiv \frac{\partial}{\partial y}\,, \quad \partial_z \equiv \frac{\partial}{\partial z}\,.$$

This set of equations of motion should be supplemented by boundary conditions. The tangential components of the stress tensor must vanish at the free surface:

$$\sigma_{xz} = 0\,, \qquad \sigma_{yz} = 0\,, \tag{2.5}$$

while the jump of the normal component of this tensor at the surface must be compensated by the capillary pressure

$$\sigma_{zz} - \sigma_{zz}^{\mathrm{ext}} - \gamma\Delta_\perp \zeta = 0\,. \tag{2.6}$$

Here, the function ζ describes the free surface displacement, σ'_{ij} is the stress tensor

$$\sigma_{ij} = -p\delta_{ij} + \sigma'_{ij} + \sigma^r_{ij}\,,$$

σ_{zz}^{ext} is the contribution from external forces, and σ'_{ij} is the viscous stress tensor.

In an incompressible smectic A, the viscous stress tensor has the form [3,5]

$$\sigma'_{ij} = 2\eta_2 v_{ij} + 2(\eta_3 - \eta_2)(v_{iz}\,\delta_{jz} + v_{jz}\,\delta_{iz}) + \eta' v_{zz}\,\delta_{iz}\,\delta_{jz}\,, \tag{2.7}$$

where

$$v_{ij} = \frac{1}{2}(\partial_i v_j + \partial_j v_i)\,,$$

and the designation

$$\eta' = \eta_1 + \eta_2 - 4\eta_3 - 2\eta_5 + \eta_4$$

is used, with η_i, $i = 1, 2, \ldots, 5$ being the coefficients of viscosity. Part of the stress tensor σ_{ij}^r related to inhomogeneous displacements of smectic layers has the following components entering into the boundary conditions [3, 5]:

$$\sigma_{zz}^r = B\,\frac{\partial u}{\partial z}\,, \quad \sigma_{xz}^r = -K\Delta_\perp \frac{\partial u}{\partial x}\,, \quad \sigma_{yz}^r = -K\Delta_\perp \frac{\partial u}{\partial y}\,.$$

The stress tensor above the free surface is determined only by the external pressure

$$\sigma_{ij}^{\text{ext}} = -p_{\text{ext}}\,\delta_{ij}\,.$$

The last boundary condition is the impermeability of the surface,

$$\frac{\partial \zeta}{\partial t} = v_z\,. \tag{2.8}$$

Equation of motion (2.3) and boundary conditions (2.5), (2.6), and (2.8) govern smectic A movements.

3. Dynamics of smectic-A films

3.1 Freely suspended films

The system of equations (2.3) that describes the motion of smectics A has been constructed in the framework of continuum mechanics. At the same time, an important role in the description of thin smectic films is attached to such structural parameters as the interlayer distance d absent in equations of continuum mechanics. This poses a problem of a consistent description of thin films, since these systems exhibit properties of a macroscopic object while small film thickness facilitates manifestation of their discrete structure.

Two models, continuous [6–12] and discrete [13–20], are currently employed to describe motions in smectic films. In the former model, which is natural to use for the description of thick films, the system of equations of smectic A motion with boundary conditions at the film surface is solved. In the discrete model, the film is regarded as a set of elastically coupled smectic layers. Therefore, it is natural to apply it to the description of thin films.

Let us begin by considering the discrete model. In the context of this model, the free energy of the film has the form

$$F = \frac{1}{2}\int \left\{ \frac{B}{d}\sum_{n=1}^{N-1}(u_{n+1} - u_n)^2 + dK\sum_{n=1}^{N}(\Delta_\perp u_n)^2 + \gamma\left[(\nabla_\perp u_1)^2 + (\nabla_\perp u_N)^2\right] \right\} \mathrm{d}\mathbf{r}_\perp\,, \tag{3.1}$$

where N is the number of layers.

In order to describe film dynamics, an equation of motion is written for each layer. In these equations, the force applied to the nth layer and referred to the unit surface is composed of elastic $-(1/d)(\delta F/\delta u_n)$ and viscous $\eta_3\Delta_\perp(\partial u_n/\partial t)$ forces [6, 12, 14]. In this case, the set of equations of motion has the form

$$\begin{aligned}
\rho\,\frac{\partial^2 u_1(\mathbf{r}_\perp,t)}{\partial t^2} &= B\,\frac{u_2(\mathbf{r}_\perp,t) - u_1(\mathbf{r}_\perp,t)}{d^2} - K\Delta_\perp^2 u_1(\mathbf{r}_\perp,t) \\
&\quad + \frac{\gamma}{d}\,\Delta_\perp u_1(\mathbf{r}_\perp,t) + \eta_3\Delta_\perp\,\frac{\partial u_1(\mathbf{r}_\perp,t)}{\partial t}\,, \\
\rho\,\frac{\partial^2 u_n(\mathbf{r}_\perp,t)}{\partial t^2} &= B\,\frac{u_{n+1}(\mathbf{r}_\perp,t) - 2u_n(\mathbf{r}_\perp,t) + u_{n-1}(\mathbf{r}_\perp,t)}{d^2} \\
&\quad - K\Delta_\perp^2 u_n(\mathbf{r}_\perp,t) + \eta_3\Delta_\perp\,\frac{\partial u_n(\mathbf{r}_\perp,t)}{\partial t}\,, \\
&\quad n = 2,3,\ldots,N-1\,, \\
\rho\,\frac{\partial^2 u_N(\mathbf{r}_\perp,t)}{\partial t^2} &= B\,\frac{u_{N-1}(\mathbf{r}_\perp,t) - u_N(\mathbf{r}_\perp,t)}{d^2} - K\Delta_\perp^2 u_N(\mathbf{r}_\perp,t) \\
&\quad + \frac{\gamma}{d}\,\Delta_\perp u_N(\mathbf{r}_\perp,t) + \eta_3\Delta_\perp\,\frac{\partial u_N(\mathbf{r}_\perp,t)}{\partial t}\,.
\end{aligned} \tag{3.2}$$

For the solution in the form of a plane wave

$$u_n(\mathbf{q}_\perp,\omega)\exp(\mathrm{i}\mathbf{q}_\perp\mathbf{r}_\perp - \mathrm{i}\omega t)\,,$$

the set of equations (3.2) is turned into a system of linear homogeneous equations for the components $u_1(\mathbf{q}_\perp,\omega), \ldots, u_N(\mathbf{q}_\perp,\omega)$. Omitting the arguments in the Fourier components, we have

$$\begin{aligned}
&\left(\rho\omega^2 + \mathrm{i}\omega\eta_3 q_\perp^2 - \frac{B}{d^2} - Kq_\perp^4 - \frac{\gamma}{d}\,q_\perp^2\right)u_1 + \frac{B}{d^2}\,u_2 = 0\,, \\
&\left(\rho\omega^2 + \mathrm{i}\omega\eta_3 q_\perp^2 - 2\frac{B}{d^2} - Kq_\perp^4\right)u_n + \frac{B}{d^2}\,u_{n-1} + \frac{B}{d^2}\,u_{n+1} = 0\,, \\
&\qquad n = 2,3,\ldots,N-1\,, \\
&\left(\rho\omega^2 + \mathrm{i}\omega\eta_3 q_\perp^2 - \frac{B}{d^2} - Kq_\perp^4 - \frac{\gamma}{d}\,q_\perp^2\right)u_N + \frac{B}{d^2}\,u_{N-1} = 0\,.
\end{aligned} \tag{3.3}$$

The set of equations (3.2) or (3.3) actually describes the motion of a bounded one-dimensional chain. It is convenient to write this system of equations in the matrix form

$$\widehat{A}\mathbf{u} = 0\,, \tag{3.4}$$

where

$$\mathbf{u} = \begin{pmatrix} u_1 \\ u_2 \\ \vdots \\ u_N \end{pmatrix},$$

$$\widehat{A} = \begin{pmatrix}
2x+1-\alpha & 1 & 0 & \ldots & 0 & 0 & 0 \\
1 & 2x & 1 & \ldots & 0 & 0 & 0 \\
0 & 1 & 2x & \ldots & 0 & 0 & 0 \\
\vdots & \vdots & \vdots & \ddots & \vdots & \vdots & \vdots \\
0 & 0 & 0 & \ldots & 2x & 1 & 0 \\
0 & 0 & 0 & \ldots & 1 & 2x & 1 \\
0 & 0 & 0 & \ldots & 0 & 1 & 2x+1-\alpha
\end{pmatrix}. \tag{3.5}$$

Here, the following designations are introduced:

$$x = -1 + \frac{d^2}{2B}\left(\rho\omega^2 + \mathrm{i}\omega\eta_3 q_\perp^2 - Kq_\perp^4\right), \qquad (3.6)$$

$$\alpha = \frac{d\gamma q_\perp^2}{B}.$$

For such systems, the problem of determining eigenmode frequencies reduces to finding the roots of the characteristic equation

$$\det \widehat{A} = 0. \qquad (3.7)$$

Characteristic equation (3.7) for films with a sufficiently large number of layers is an algebraic equation of a high power in ω^2. It is convenient to solve this equation by the method based on the relationship between Chebyshev polynomials of the second kind, $U_n(x)$, and tridiagonal symmetric determinants of the nth order [21, 22]:

$$U_n(x) = \begin{vmatrix} 2x & 1 & 0 & \ldots & 0 & 0 & 0 \\ 1 & 2x & 1 & \ldots & 0 & 0 & 0 \\ 0 & 1 & 2x & \ldots & 0 & 0 & 0 \\ \vdots & \vdots & \vdots & \ddots & \vdots & \vdots & \vdots \\ 0 & 0 & 0 & \ldots & 2x & 1 & 0 \\ 0 & 0 & 0 & \ldots & 1 & 2x & 1 \\ 0 & 0 & 0 & \ldots & 0 & 1 & 2x \end{vmatrix}. \qquad (3.8)$$

Characteristic equation (3.7) is an equation with respect to x (3.6)

$$[x + 1 - \alpha]\, U_{N-1}(x) - \alpha\left(1 - \frac{\alpha}{2}\right) U_{N-2}(x) = 0. \qquad (3.9)$$

Each root of this equation, $x^{(l)}$, yields two eigenfrequencies

$$\omega_\pm^{(l)} = -\mathrm{i}\frac{\eta_3 q_\perp^2}{2\rho} \pm \sqrt{\frac{2B}{\rho d^2}\left(1 + x^{(l)}\right) + \frac{Kq_\perp^4}{\rho} - \frac{\eta_3^2 q_\perp^4}{4\rho^2}},$$

$$l = 1, 2, \ldots, N. \qquad (3.10)$$

An advantage of using Chebyshev polynomials is that a relatively simple trigonometric equation may be solved instead of an algebraic characteristic equation (3.7) of power N with respect to x. Such a possibility ensues from the trigonometric representation of the Chebyshev polynomials [21, 22]:

at $|x| \leqslant 1$,

$$x = \cos\theta, \qquad U_n(\cos\theta) = \frac{\sin\left[(n+1)\,\theta\right]}{\sin\theta}; \qquad (3.11)$$

at $x \geqslant 1$,

$$x = \cosh\theta, \qquad U_n(\cosh\theta) = \frac{\sinh\left[(n+1)\,\theta\right]}{\sinh\theta}; \qquad (3.12)$$

at $x \leqslant -1$,

$$x = -\cosh\theta, \quad U_n(-\cosh\theta) = (-1)^n \frac{\sinh\left[(n+1)\theta\right]}{\sinh\theta}. \qquad (3.13)$$

The use of representation (3.11) leads to a characteristic equation of the form

$$(1 - \alpha + \cos\theta)\,\frac{\sin(N\theta)}{\sin\theta} = \alpha\left(1 - \frac{\alpha}{2}\right)\frac{\sin\left[(N-1)\,\theta\right]}{\sin\theta}, \qquad (3.14)$$

where $0 \leqslant \theta \leqslant \pi$. It follows from Eqn (3.7) that in the range of $0 \leqslant \alpha \leqslant 2$ all N roots of Eqn (3.3) are real and lie within the limits $|x_l| \leqslant 1$. At typical parameter values of smectic A [1, 2]

$$d \sim 30\,\text{Å}, \quad \gamma \sim 30\ \text{erg cm}^{-2}, \quad B \sim 2.5 \times 10^7\ \text{erg cm}^{-3},$$

the condition that $\alpha \leqslant 2$ is fulfilled for wave vectors $q_\perp \leqslant 2 \times 10^6\ \text{cm}^{-1}$; in other words, it covers the entire range of transverse components of the wave vector examined in wave scattering experiments. Note that the range of $q_\perp$ values is substantially extended in systems with a large elasticity constant $B \sim 10^8 - 10^9\ \text{erg cm}^{-3}$. The solution of characteristic equation (3.9) at small α values in the lowest order in α has the form

$$x^{(1)} = -1 + \frac{\alpha}{N}, \; x^{(l)} = -\cos\frac{(l-1)\pi}{N} + 2\,\frac{\alpha}{N}\cos^2\frac{(l-1)\pi}{2N},$$

$$l = 2, 3, \ldots, N. \qquad (3.15)$$

At $q_\perp \to 0$, all eigenmotions of the film are vibrational, with vibration frequencies having the form, according to (3.10),

$$\omega_\pm^{(1)} = \pm c^{(1)} q_\perp - \mathrm{i}\omega'', \qquad (3.16)$$

$$\omega_\pm^{(l)} = \pm\frac{c^{(l)}}{d} - \mathrm{i}\omega'', \qquad l = 2, 3, \ldots, N,$$

where

$$c^{(1)} = \sqrt{\frac{2\gamma}{\rho dN}}, \qquad (3.17)$$

$$c^{(l)} = 2\sqrt{\frac{B}{\rho}}\sin\frac{l\pi}{2N}, \qquad l = 2, 3, \ldots, N,$$

$$\omega'' = \frac{\eta_3 q_\perp^2}{2\rho}.$$

The first mode $\omega_\pm^{(1)}$ is a transverse acoustic wave spreading under the effect of surface tension forces. In the remaining modes, the frequency of vibrations at $q_\perp \to 0$ is independent of $q_\perp$; in other words, these are optical modes. As $q_\perp$ values grow, the vibrational modes undergo successive transformations to relaxation modes starting from the first one, $l = 1$, which becomes relaxational at

$$q_\perp^2 > \frac{8\gamma\rho}{\eta_3^2 dN}. \qquad (3.18)$$

In this case, the relaxation time for the first mode $\tau_+^{(1)}$ very rapidly attains a constant value

$$\tau_+^{(1)} = \frac{\eta_3 Nd}{2\gamma}, \qquad (3.19)$$

which is significantly larger than the relaxation times of all other modes at small α.

The amplitude of film displacements in each mode can be found from the solution of the homogeneous set of equations (3.4). The solution to Eqn (3.4) yields

$$u_n^{(l)}(q_\perp) = (-1)^{n-1}\left[U_{n-1}(x^{(l)}) + (1-\alpha)\,U_{n-2}(x^{(l)})\right],$$
$$n, l = 1, 2, ..., N, \tag{3.20}$$

where the first-layer displacement amplitude is assumed to be equal to unity and formally $U_{-1}(x) = 0$ and $U_0(x) = 1$. Figure 1 shows the types of layer motion in a six-layer film for each mode.

An arbitrary motion in a smectic film can be represented in the form of an expansion in terms of normal layer fluctuations

$$u_n(\mathbf{r}_\perp, t) = \mathrm{Re}\int \exp(\mathrm{i}\mathbf{q}_\perp\mathbf{r}_\perp)\sum_{l=1}^{N}\left[a_+^{(l)}(\mathbf{q}_\perp)\exp(-\mathrm{i}\omega_+^{(l)}t)\right.$$
$$\left. + a_-^{(l)}(\mathbf{q}_\perp)\exp(-\mathrm{i}\omega_-^{(l)}t)\right]u_n^{(l)}(\mathbf{q}_\perp)\frac{\mathrm{d}\mathbf{q}_\perp}{(2\pi)^2}, \quad n = 1, 2, ..., N. \tag{3.21}$$

Here, $a_\pm^{(l)}(\mathbf{q}_\perp)$ are complex eigenmode amplitudes.

The main type of low-frequency motions of a freely suspended film is acoustic fluctuations that have no effect on interlayer distances. Studies of these fluctuations yield information about the coefficient of surface tension γ at the smectic's free boundary. Traditional methods used to study ordinary fluids are hardly applicable to smectics, in which strain-related bulk stresses are comparable to surface ones. A method for measuring γ by excitation of acoustic fluctuations was proposed and implemented in Ref. [23].

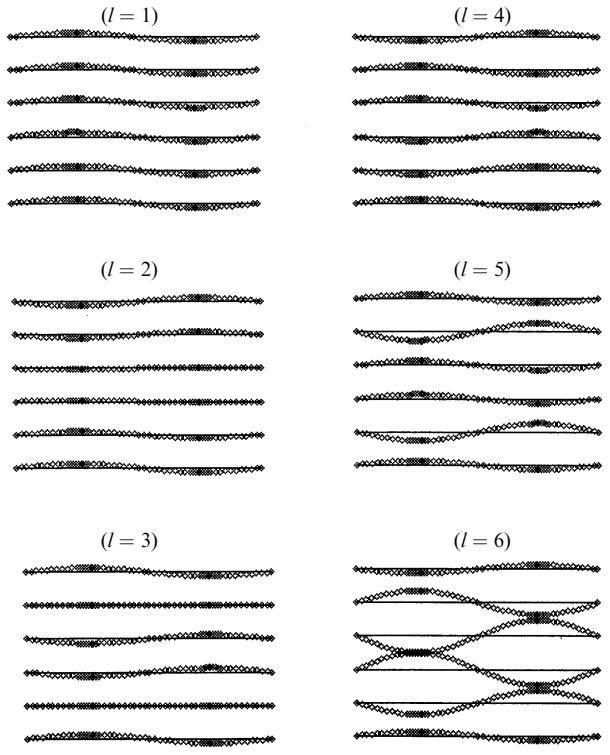

Figure 1. Types of eigenmodes for a free-standing six-layer smectic-*A* film. Acoustic mode: $l = 1$; optical modes: $l = 2, 3, \ldots, 6$ [19].

Transverse motion of film as a whole was described by the equation

$$\rho L\frac{\partial^2 u}{\partial t^2} = 2\gamma\Delta_\perp u, \tag{3.22}$$

where L is the film thickness. In [23], the film was a round membrane of radius R. The solution of Eqn (3.22) in this case had the form

$$u(r_\perp, \varphi, t) = J_n(kr_\perp)\exp(\mathrm{i}n\phi)\,\exp(-\mathrm{i}\omega t), \tag{3.23}$$

where $J_n(x)$ is the Bessel function, n is an integer, φ is the polar angle, and

$$k = \omega\sqrt{\frac{\rho L}{2\gamma}}. \tag{3.24}$$

The eigenmode spectrum for a supported film is found from the boundary condition $u(R, \varphi, t) = 0$, i.e., $J_n(Rk) = 0$.

The damping of film fluctuations is due to internal friction or viscosity and is also related to the interaction with air, the contribution of which is described by the parameter

$$\delta \sim \frac{p}{\rho L\bar{u}\omega},$$

where $\bar{u}$ is the average velocity of the gas molecules. In order to diminish fluctuation damping, the measurements were made in a helium-filled cell. Helium was chosen because, for a given pressure, the thermal velocity of its atoms was much higher, hence δ was smaller.

The study was conducted with a BBOA liquid-crystal film of thickness $L = 4850$ Å and radius $R = 0.4$ cm at a temperature $T = 45°$C and a pressure $p = 40$ mTorr. Membrane fluctuations were generated by an electrical pulse, and the eigenfrequency spectrum was detected by specularly reflecting a laser beam. The oscillation amplitude was found to be around 10 Å. The fluctuation spectrum is presented in Fig. 2.

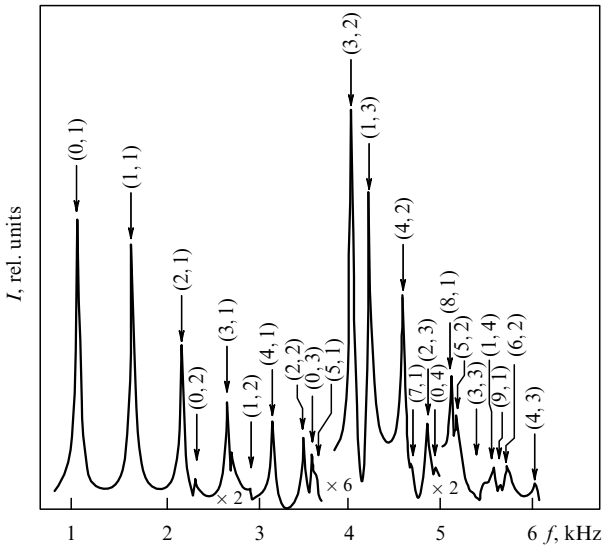

Figure 2. Vibrational modes in a freely suspended BBOA smectic film of thickness 4850 Å and radius $R = 0.4$ cm at a temperature of 45 °C and a pressure of 40 mTorr. The numerals in the parentheses (n, m) designate the mth root of the Bessel function of order n. Arrows indicate the frequencies calculated with a single adjustable parameter assuming $\gamma = 27$ dyn cm^{-1} [23].

Surface tension was $\gamma = 27$ dyn cm^{-1}. This value was deduced from the analysis of the first five low-frequency eigenmodes (0,1), (1,1), (2,1), (0,2), and (3,1), where the first figure labels the order of the Bessel function and the second one is the index of the wave-number eigenvalue. For higher-frequency modes, an appreciable contribution to the right-hand side of equation of motion (3.22) is made by the bulk forces described in an elastic medium by the term

$$\frac{-EL^3}{\left[12(1-\sigma^2)\right]}\,\Delta_\perp^2 u\,,$$

where E is Young's modulus and σ is the Poisson ratio. In smectics, this corresponds to the term $-K\Delta_\perp^2 u$ in the system of equations (3.2).

It has been demonstrated that surface tension has no peculiarities at smectic-A – smectic-B transition temperature $T_{AB} = 49.5\,^\circ$C in the bulk phase and is significantly decreased at temperatures 5–10 K above T_{AB}.

Another method for measuring surface tension in freely suspended thin films was proposed and applied in Refs [24, 25]. In this method, one of the lateral sides of the frame was a very thin filament with a load. The surface tension of the film is related to the curvature radius of the filament R as follows:

$$R = \frac{m_\mathrm{w} g}{2\gamma} + \frac{f_\mathrm{fr}}{2\gamma}\,,$$

where m_w is the mass of the load, f_fr is the frictional force in the gap, and g is the acceleration of gravity. In Refs [24, 25], $R \sim 5$ cm, $m_\mathrm{w} \sim 0.2$ g, and the friction-determined contribution was negligibly small.

The measurements were made using 650BC and H(10)F(5)MOOP smectics A. It was shown that in either case, a change of the film thickness from 100 to 2 layers failed to affect surface tension up to the error of this technique. The H(10)F(5)MOOP film was additionally examined for the temperature dependence of surface tension, which was found to undergo no variation in a range from 74 to 84 °C.

3.2 Solid-supported films

Apart from free-standing films, solid-supported films (fastened to a substrate) are also of interest. The description of their properties in the framework of the discrete model proceeds from the above expression for the free energy of the film (3.1) on the assumption of a zero displacement of the last (fastened) layer $u_N = 0$. The same refers to the set of equations of motion (3.2). In the Fourier representation in the matrix form, the system of equations of motion for a supported film looks like [26]

$$\widehat{A}_\mathrm{s}\mathbf{u} = 0\,, \tag{3.25}$$

where

$$\mathbf{u} = \begin{pmatrix} u_1 \\ u_2 \\ \vdots \\ u_{N-1} \end{pmatrix},$$

$$\widehat{A}_\mathrm{s} = \begin{pmatrix} 2x+1-\alpha & 1 & 0 & \ldots & 0 & 0 \\ 1 & 2x & 1 & \ldots & 0 & 0 \\ 0 & 1 & 2x & \ldots & 0 & 0 \\ \vdots & \vdots & \vdots & \ddots & \vdots & \vdots \\ 0 & 0 & 0 & \ldots & 2x & 1 \\ 0 & 0 & 0 & \ldots & 1 & 2x \end{pmatrix}. \tag{3.26}$$

In this case, the condition for the existence of a nonzero solution to Eqn (3.25) $\det \widehat{A}_\mathrm{s} = 0$ has the form

$$U_{N-1}(x) + (1-\alpha)\,U_{N-2}(x) = 0\,. \tag{3.27}$$

In the case of small wave numbers, $q_\perp \ll \sqrt{B/(\gamma d)}$, in the lowest order in α, for the roots of characteristic equation (3.27), we have

$$x^{(l)} = -\cos\frac{(2l-1)\pi}{2N-1} + \frac{2\alpha}{2N-1}\cos^2\frac{(2l-1)\pi}{2(2N-1)}\,,$$

$$l = 1, 2, \ldots, N-1\,. \tag{3.28}$$

The set of eigenfrequencies of a supported film is obtained from the same equation (3.6) as for a freely suspended one. As a result, we obtain

$$\omega_\pm^{(l)} = -\mathrm{i}\,\frac{\eta_3 q_\perp^2}{2\rho} \pm \left[\frac{4B}{\rho d^2}\sin^2\frac{(2l-1)\pi}{2(2N-1)} + \frac{4\gamma q_\perp^2}{(2N-1)\rho d}\cos^2\frac{(2l-1)\pi}{2(2N-1)} - \frac{\eta_3^2 q_\perp^4}{4\rho^2}\right]^{1/2}. \tag{3.29}$$

At $q_\perp^2 < \pi\sqrt{B}/(\eta_3 N d)$, all eigenmotions of the film are vibrational. When $q_\perp$ increases, as in freely suspended films, all the modes become relaxation modes, starting from the first one. A distinct peculiarity of the dynamics of supported films is the absence of an acoustic mode and a relatively weak influence of surface tension on film dynamics, which largely depends on bulk forces.

Analysis of eigenmodes for supported films has shown that they are not separated into optical and acoustic ones. The centers of mass undergo a shift regardless of the type of fluctuations, and their frequency for all modes remains finite at $q \to 0$.

The layer-displacement amplitudes during normal vibrations of smectic films fastened to a flat surface are given by Eqn (3.20) as before, with the only difference that the Nth layer remains motionless.

4. Continuous model

4.1 Comparison of continuous and discrete models

In the framework of the continuous model, a film of incompressible liquid crystal is regarded as a continuum with a free energy (2.1)–(2.2). Layer-displacement dynamics is described by the equation [12]

$$\rho\,\frac{\partial^2 u}{\partial t^2} = \eta_3\Delta_\perp\frac{\partial u}{\partial t} + B\,\frac{\partial^2 u}{\partial z^2} - K\Delta_\perp^2 u \tag{4.1}$$

with the boundary conditions at the film surface

$$-\gamma\Delta_\perp\left[u\left(\mathbf{r}_\perp, z = \pm\frac{L}{2}, t\right)\right] \pm B\,\frac{\partial u(\mathbf{r}_\perp, z = \pm L/2, t)}{\partial z} = 0\,. \tag{4.2}$$

Equation (4.1) does not take into account the permeation effect, which has practically no influence on layer displacements as shown in [6, 11, 27]. The boundary condition (4.2) is written on the assumption that dissipative processes at the surfaces can be neglected; it has the sense of an elastic-force balance.

After passing to Fourier representation in terms of time t and transverse variable $\mathbf{r}_\perp$, we found from (4.1) and (4.2) that the eigenfrequencies of film fluctuations are

$$\omega_\pm = -\frac{i\eta_3 q_\perp^2}{2\rho} \pm \sqrt{\frac{\lambda B}{\rho} + \frac{Kq^4}{\rho} - \frac{\eta_3^2 q_\perp^4}{4\rho^2}}, \tag{4.3}$$

where λ are the eigenvalues of the Sturm – Liouville problem for the equation

$$\frac{\partial^2 u}{\partial z^2} + \lambda u = 0$$

with boundary conditions

$$B\,\frac{\partial u\,(z = \pm L/2)}{\partial z} \pm \gamma q_\perp^2 u\left(z = \pm\frac{L}{2}\right) = 0\,.$$

The equation that defines the eigenvalues λ has the form [11, 12]

$$\tan(w\beta) = \frac{2\beta}{\beta^2 - 1}\,, \tag{4.4}$$

where

$$\beta^2 = \lambda\,\frac{B^2}{\gamma^2 q_\perp^4}\,, \qquad w = \frac{\gamma L q_\perp^2}{B}\,. \tag{4.5}$$

Equation (4.5) has an infinite number of real positive roots that can be found numerically, while formula (4.4) describes the eigenfrequency spectrum of the film.

For cases $q_\perp^2 \ll B/(\gamma L)$ and $q_\perp^2 \gg B/(\gamma L)$, approximate solutions of Eqn (4.4) can be found. In particular, for the most interesting case of small wave numbers, the continuous model leads to the following infinite set of eigenfrequencies:

$$\omega_1^\pm = -i\,\frac{\eta_3 q_\perp^2}{2\rho} \pm \frac{\eta_3 q_\perp^2}{2\rho}\sqrt{\frac{4\rho}{\eta_3^2}\left[K + \frac{\gamma^2}{B}\left(\frac{2B}{\gamma L q_\perp^2} - \frac{1}{3}\right)\right] - 1}\,,$$

$$\omega_l^\pm = -i\,\frac{\eta_3 q_\perp^2}{2\rho} \pm \frac{\eta_3 q_\perp^2}{2\rho}\sqrt{\frac{4\rho}{\eta_3^2}\left[K + \frac{\gamma^2}{B}\left(\frac{\pi B(l-1)}{\gamma L q_\perp^2} + \frac{2}{\pi(l-1)}\right)^2\right] - 1}\,,$$

$$l = 2, 3, 4, \ldots$$

It should be emphasized that the continuous and discrete approaches to the description of film dynamics are essentially different. Indeed, the former disregards the discrete nature of smectic films, assuming that there is no interlayer distance d among film parameters. Formally, it makes this approach incorrect for the description of thin films. In the discrete approach, the layered film structure is explicitly taken into consideration, which makes it especially convenient for the description of properties of thin films. The continuous and discrete approaches use different equations, boundary conditions, and methods of their solution for the description of film dynamics. In many cases, however, the two approaches give similar results. It has been noted in [12] that this may be due to the large degree of concordance between their equations despite their apparent difference.

The two approaches may be compared by showing how the equations of the discrete model are derived from the equations of the continuous one. In the latter, film dynamics is described by Eqn (4.1) with the boundary conditions (4.2) at the film surface. Let us break down a film into $N+1$ intervals of thickness d along axis z and substitute derivatives with respect to z by their discrete analogs. Then, Eqn (4.1) gives the system of equations

$$\rho\,\frac{\partial^2 u_N}{\partial t^2} = \eta_3\Delta_\perp\,\frac{\partial u_n}{\partial t} + B\,\frac{u_{n+1} - 2u_n + u_{n-1}}{d^2} - K\Delta_\perp^2 u_n\,, \qquad n = 1, 2, \ldots, N\,,$$

$$\frac{u_{N+1} - u_N}{d} - \frac{\gamma}{B}\,\Delta_\perp u_N = 0\,,$$

$$\frac{u_1 - u_0}{d} + \frac{\gamma}{B}\,\Delta_\perp u_1 = 0\,.$$

Using the last two equalities to exclude u_{N+1} and u_0, the following system of equations is obtained for displacements $u_1, u_2, \ldots, u_N$:

$$\rho\,\frac{\partial^2 u_1}{\partial t^2} = \eta_3\Delta_\perp\,\frac{\partial u_1}{\partial t} + B\,\frac{u_2 - 2u_1}{d^2} - K\Delta_\perp^2 u_1 + \frac{B}{d^2}u_1 + \frac{\gamma}{d}\,\Delta_\perp u_1\,,$$

$$\rho\,\frac{\partial^2 u_n}{\partial t^2} = \eta_3\Delta_\perp\,\frac{\partial u_n}{\partial t} + B\,\frac{u_{n+1} - 2u_n + u_{n-1}}{d^2} - K\Delta_\perp^2 u_n\,, \qquad n = 2, 3, \ldots, N-1\,,$$

$$\rho\,\frac{\partial^2 u_N}{\partial t^2} = \eta_3\Delta_\perp\,\frac{\partial u_N}{\partial t} + B\,\frac{u_{N-1} - 2u_N}{d^2} - K\Delta_\perp^2 u_N + \frac{B}{d^2}\,u_N + \frac{\gamma}{d}\,\Delta_\perp u_N\,.$$

If N is the number of layers in the film and d is the equilibrium distance between smectic layers, this system of equations coincides with system (3.2) used as the starting point in the discrete approach.

Comparison of eigenfrequencies obtained from discrete (3.10) and continuous (4.3) models indicates that the two yield virtually identical results for the acoustic mode. A small difference between eigenfrequencies appears as the mode index grows.

4.2 Surface fluctuations

Structural peculiarities of smectic liquid crystals are manifested them selves in their surface properties. It is known that in solids, where the main role is played by bulk forces, surface fluctuations are elastic waves [3]. In liquids, where surface tension is of greater importance, surface fluctuations are represented either by capillary waves or by motions damped under the effect of viscous stress [28]. Because smectics are intermediate between liquids and crystalline solids, their motions reflect properties of both these states.

In the description of surface motions, smectics may be regarded as incompressible. Moreover, as mentioned in the foregoing, the permeation effect may be disregarded, i.e., $v_z = \partial u/\partial t$. In this case, surface fluctuations are defined by the following system of equations of motion [3, 28]

$$\frac{\partial v_x}{\partial x} + \frac{\partial v_z}{\partial z} = 0\,,$$

$$\rho\,\frac{\partial v_i}{\partial t} = -\partial_i p + \partial_j\sigma'_{ij} + \left[B\,\frac{\partial^2 u}{\partial z^2} - K\left(\frac{\partial^2}{\partial x^2}\right)^2 u\right]\delta_{iz}\,, \quad i = x, z\,,$$

$$v_z = \frac{\partial u}{\partial t} \tag{4.6}$$

with boundary conditions

$$\lim_{z\to-\infty} v_i = 0\,, \qquad i = x, z\,,$$
$$-K\frac{\partial^3 u}{\partial x^3} + \eta_3\left(\frac{\partial v_x}{\partial z} + \frac{\partial v_z}{\partial x}\right) = 0\,, \tag{4.7}$$
$$p^{\text{ext}} - p + B\frac{\partial u}{\partial z} + (\eta_1 - \eta_2 + \eta_4 - 2\eta_5)\frac{\partial v_z}{\partial z} - \gamma\frac{\partial^2\zeta}{\partial x^2} = 0\,,$$

which are the conditions of surface-wave damping with depth, of the zero tangential component of the stress tensor, $\sigma_{xz} = 0$, and of compensation of the jump of the stress-tensor normal component by surface capillary forces, respectively.

It is assumed that a smectic liquid crystal in equilibrium occupies the half-space $z \leqslant 0$ and that the surface-wave motion is uniform along the y axis and occurs in the xz plane. Function ζ describes free surface displacement and p is pressure.

It is convenient to find the solution to Eqns (4.6) and (4.7) in the form of plane waves

$$\exp(q_z z + \mathrm{i}q_\perp x - \mathrm{i}\omega t)\,.$$

In this case, the condition for the existence of a nonzero solution of system (4.6) has the form [6, 29]

$$\mathrm{i}\omega\tau_{\mathrm{M}} S^4 + \left[1 - \mathrm{i}\omega\tau_{\mathrm{M}}\left(2 + \frac{\eta'}{\eta_3}\right) - \frac{\omega^2}{c_2^2 q^2}\right] S^2 - \left(\lambda^2 q^2 - \mathrm{i}\omega\tau_{\mathrm{M}} - \frac{\omega^2}{c_2^2 q^2}\right) = 0\,, \tag{4.8}$$

where the following designations are used:

$$S = \frac{q_z}{q_\perp}\,, \qquad \lambda = \sqrt{\frac{K}{B}}\,,$$
$$\eta' = \eta_1 + \eta_2 - 4\eta_3 - 2\eta_5 + \eta_4\,,$$
$$\tau_{\mathrm{M}} = \frac{\eta_3}{B}$$

is the Maxwell relaxation time, and $c_2 = \sqrt{B/\rho}$ is the characteristic velocity of the second sound in smectic A.

Equation (4.8) at given $q_\perp$ and ω can be used to derive S and, hence, the law of surface-wave damping with depth. Because only two of the four roots of Eqn (4.8) correspond to decreasing solutions, $\mathrm{Re}\, S_{1,2} > 0$, the displacement u in the surface wave can be represented as

$$u = \exp(\mathrm{i}q_\perp x - \mathrm{i}\omega t)\left[u_1\exp(S_1 q_\perp z) + u_2\exp(S_2 q_\perp z)\right]. \tag{4.9}$$

Then, the boundary conditions (4.7) have the form

$$\sum_{k=1}^{2}\left[\eta_3\omega(S_k^2 + 1) + \mathrm{i}Kq^2\right] q u_k = 0\,, \tag{4.10}$$
$$\sum_{k=1}^{2}\left\{BS_k q + \gamma q^2 - \left[\omega\rho + \mathrm{i}\eta_3(3 - S_k^2)q^2 + \mathrm{i}\eta' q^2\right]\frac{\omega S_k}{q}\right\} u_k = 0\,. \tag{4.11}$$

They make up a system of equations that define the relationship between the amplitudes of modes corresponding to roots S_1 and S_2. The condition for the existence of nonzero solutions of system (4.10)–(4.11) leads to a dispersion equation relating $q_\perp$ to ω. It was analyzed in [6, 11] for a smectic layer and in [29] for a semi-infinite medium.

In the frequency range $|\omega| \ll 1/\tau_{\mathrm{M}}$, there exist surface eigenmodes with the dispersion law

$$\omega = \pm c_2 q_\perp - \mathrm{i}\sqrt{\frac{\eta_3 c_2}{8\rho}}\, q_\perp^{3/2}\,. \tag{4.12}$$

Component q_z that governs damping of surface waves with the depth in the medium is derived from the relation

$$q_z^4 = \mathrm{i}\,\frac{\omega\rho}{\eta_3}\, q_\perp^2\,. \tag{4.13}$$

Equation (4.12) corresponds to waves analogous to the Rayleigh waves at the surface of an isotropic solid. These waves are substantially different from the second-sound wave known to exist in the bulk phase [30]. To begin with, they can propagate parallel to the smectic layers, unlike the second-sound wave in the bulk. Moreover, the velocity of surface waves $c_2 = \sqrt{B/\rho}$ is twice the maximum velocity of the second sound.

At frequencies $|\omega| \sim 1/\tau_{\mathrm{M}}$, the oscillatory regime is replaced by the relaxation one. At $|\omega| \gg 1/\tau_{\mathrm{M}}$, the surface motion becomes purely relaxational, with the dispersion law

$$\omega = -\mathrm{i}\,\frac{4\eta_3 q_\perp^2}{3\rho}\,. \tag{4.14}$$

These modes decay with depth as in usual isotropic fluids:

$$q_{z,1} = q_\perp\,, \qquad q_{z,2} = q_\perp\sqrt{1 - \mathrm{i}\,\frac{\omega\rho}{\eta_3 q^2}}\,. \tag{4.15}$$

Two main types of surface motions were identified in the bounded specimens studied in Ref [6]. One of them was a transverse acoustic wave with a dispersion law as in thin films (3.16) and (3.17). The second mode was analogous to the first of the optical vibrations in which the specimen surfaces moved in opposite directions. Its dispersion law had the form [6]

$$\omega = \frac{2\pi^2\sqrt{KB}}{\eta_3 L\sqrt{(K/B)\,L^2 q_\perp^4 + 4\pi^2(K\rho/\eta_3^2)}}\,. \tag{4.16}$$

At $q \to 0$, this formula turns to (3.16) and (3.17) for a mode with $l = 2$. Note that these types of motion are lacking in a semi-infinite specimen where surface fluctuations are analogous to the motions of surface layers in a film on a substrate.

Recently, there has been ever increasing interest in surface fluctuations in liquids [31–35]. Surface fluctuation spectra in polymer solutions were most extensively studied, taking advantage of the possibility of modulating frequency-dependent shear viscosity i.e., viscoelastic properties of the system, by many orders of magnitude by varying the concentration of the solution practically without altering surface tension γ. Surface fluctuations were studied by optical methods, that is, from spectral characteristics of scattered light [31–35], and by applying an external force to excite surface waves [34].

It was shown experimentally that a rise in polymer concentration and, hence, in complex shear viscosity, leads

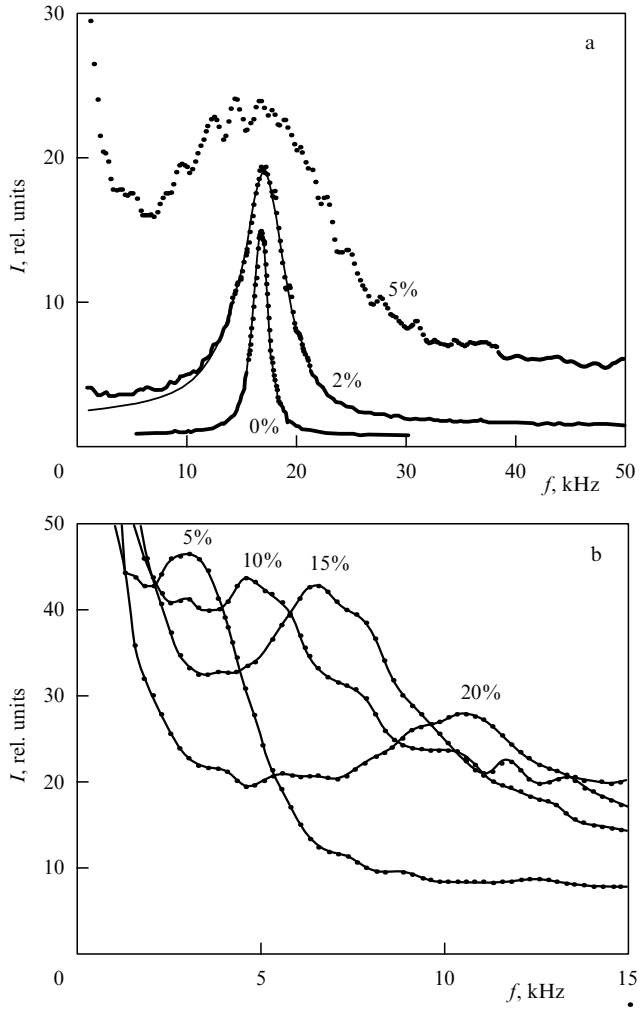

Figure 3. Power spectra of light scattered by surface fluctuations for solutions of polyisobutylene in hexane at (a) 0, 2, and 5 wt% and scattering vector $q = 742.5$ cm^{-1} or (b) 5, 10, 15, and 20 wt% and scattering vector $q = 247.5$ cm^{-1}. The solid lines in (a) are fits to the full capillary wave power spectra [31].

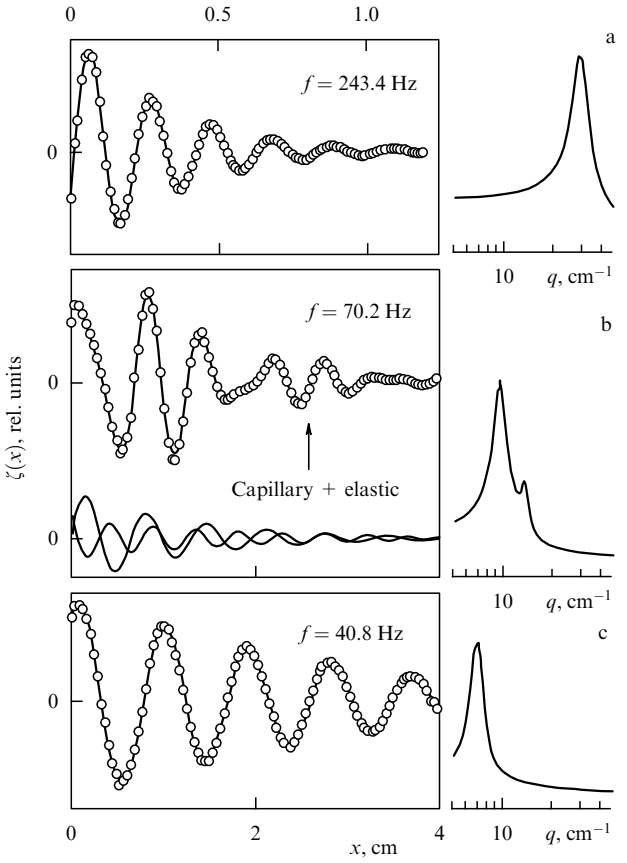

Figure 4. Crossover from (a) fully capillary waves to (c) purely Rayleigh waves with decreasing excitation frequency. (b) Both types of fluctuations occur at 70.2 Hz. Fourier transformations of the experimental profiles are represented on the right [34]. \

to the crossover from capillary wave to Rayleigh elastic mode. This transition is illustrated by Fig. 3 showing the frequency dependence of scattered light intensity at different concentrations of the solution. At low concentrations, a distinct peak is apparent at frequency $\omega_c = (\gamma q^3/\rho)^{1/2}$, whose position depends on surface tension and is therefore constant. This peak corresponds to capillary waves. As the polymer concentration increases, this peak begins to shift to higher frequencies even though γ remains unaltered. Such a behavior suggests transition from capillary waves to Rayleigh waves with the dispersion law $\omega = c_E q$, where c_E is the velocity of Rayleigh waves, which depends on the viscoelastic properties of the system.

Reference [34] reports on the crossover from elastic waves to capillary ones in a gel with a rise in exciting voltage. Interestingly, both types of motions could be observed. This transition is shown in Fig. 4. Optical studies revealed a relaxation mode of unknown nature, besides capillary waves and Rayleigh waves.

No similar studies for the surfaces of smectic liquid crystals have been carried thus far, although they are doubtlessly of great interest as a source of extensive information about elastic and viscous properties of smectic films.

5. Thermal fluctuations of smectic films

5.1 Freely suspended films

Spectral densities of smectic layer-displacement fluctuations can be found with the help of the fluctuation–dissipation theorem (FDT) [36]. For this purpose, the following term is included in expression (3.1) for the free energy:

$$F_{\text{ext}} = -\int \sum_{n=1}^{N} u_n(\mathbf{r}_\perp, t) f_n(\mathbf{r}_\perp, t)\, \mathrm{d}\mathbf{r}_\perp . \tag{5.1}$$

This term is connected with the external forces $f_n(\mathbf{r}_\perp, t)$, $n = 1, 2, \ldots, N$ that act on each layer and have the dimension of pressure. As a result, a term

$$-\frac{1}{d}\,\frac{\delta F_{\text{ext}}}{\delta u_n} = f_n ,$$

is added to the external force acting on the nth layer in equations of smectic motion.

The system of equations of motion for a freely suspended film then assumes the form

$$\widehat{A}\mathbf{u} = -\frac{d}{B}\,\mathbf{f} . \tag{5.2}$$

The solution of this system yields

$$\mathbf{u} = \hat{\chi}\,\mathbf{f}\,, \tag{5.3}$$

where the susceptibility matrix $\hat{\chi}$ is given by the expression [4, 19]

$$\chi_{nm} = \chi_{mn} = (-1)^{n+m+1}\,\frac{d}{B} \times \frac{[U_{m-1}(x) + (1-\alpha)U_{m-2}(x)]}{U_N(x) + 2(1-\alpha)U_{N-1}(x) + (1-\alpha)^2 U_{N-2}(x)} \times \left[U_{N-n}(x) + (1-\alpha)U_{N-n-1}(x)\right], \tag{5.4}$$

where

$$m, n = 1, 2, \ldots, N, \qquad n \geqslant m\,.$$

According to the FDT, the spectral densities of displacement fluctuations have the form

$$\left(u_n(\mathbf{q}_\perp)\,u_m(-\mathbf{q}_\perp)\right)_\omega = \mathrm{i}\,\frac{k_\mathrm{B}T}{\omega}\left[\chi^*_{mn}(\mathbf{q}_\perp, \omega) - \chi_{nm}(\mathbf{q}_\perp, \omega)\right]. \tag{5.5}$$

In order to calculate spatial correlation functions $\langle u_n(\mathbf{r}_\perp)\,u_m(0)\rangle$ of a freely suspended film, it is convenient to use the free energy representation in the matrix form

$$F = \frac{1}{2}\int \sum_{n,m=1}^{N} u_n(\mathbf{q}_\perp)\,M_{nm}\,u_m(-\mathbf{q}_\perp)\,\frac{\mathrm{d}\mathbf{q}_\perp}{(2\pi)^2}\,, \tag{5.6}$$

where matrix $\hat{M}$ is proportional to matrix $\hat{A}$ at a zero frequency:

$$\hat{M} = -\frac{B}{d}\,\hat{A}(\omega = 0)\,. \tag{5.7}$$

Then, the spatial correlation function has the form

$$\left\langle u_n(\mathbf{r}_\perp)\,u_m(\mathbf{0})\right\rangle = \frac{k_\mathrm{B}T}{(2\pi)^2}\int \left(\hat{M}^{-1}\right)_{nm}\exp(\mathrm{i}\mathbf{q}_\perp\,\mathbf{r}_\perp)\,\mathrm{d}\mathbf{q}_\perp\,. \tag{5.8}$$

Integration over $q_\perp$ is performed in the range $2\pi/L_\mathrm{s} < q_\perp < 2\pi/a$, where L_s is the linear size of the film surface and a is the molecular diameter.

The inverse matrix $\hat{M}^{-1}$ coincides with the susceptibility matrix at a zero frequency:

$$\hat{M}^{-1} = \hat{\chi}(\omega = 0)\,. \tag{5.9}$$

In the range of small wave numbers ($q_\perp \to 0$), all elements of the matrix $\hat{M}^{-1}$ become identical:

$$\left(\hat{M}^{-1}\right)_{nm} \approx \frac{1}{2\gamma q_\perp^2}\,. \tag{5.10}$$

At large $q_\perp$, all matrix elements rapidly decay:

$$\left(\hat{M}^{-1}\right)_{nm} \sim \frac{1}{q_\perp^{4(|n-m|+1)}}\,. \tag{5.11}$$

Figure 5 shows calculated squared layer displacements $\langle u_n^2\rangle$ in films of different thickness depending on the layer index [4]. It can be seen that thermal layer displacements in smectic films amount to approximately 10–15% of the interlayer distance. At typical parameters of a liquid crystal, the surface-layer fluctuations are suppressed by surface-tension forces. It was computed that the correlation function $\langle u_n(0)\,u_m(0)\rangle$ for inner layers decreases with growing $|n-m|$ much faster than for external ones. The decay of the correlation function $\langle u_n(0)\,u_m(\mathbf{r}_\perp)\rangle$ at large distances was found to be unrelated to layer indices n and m; the typical correlation length was on the order of $10a$, where a is the molecular diameter.

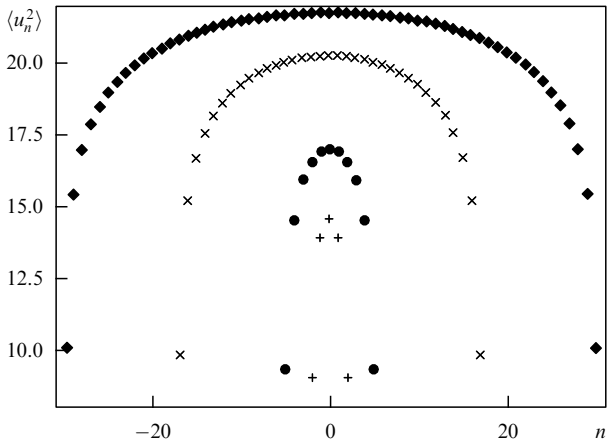

Figure 5. Calculated squared-fluctuation profiles of smectic-layer displacements vs the layer index n for films of different thickness containing 61, 35, 11, and 5 layers (from top to bottom); $n = 0$ corresponds to the center of the film. For the purpose of computation, it was assumed that $B = 2.5 \times 10^7$ dyn cm^{-2}, $K = 10^{-6}$ dyn, and $\gamma = 30$ dyn cm^{-1} [4].

5.2 Films on a substrate

For films fastened to a substrate, the susceptibility matrix $\hat{\chi}$ is found in the same way as for freely suspended films:

$$\chi_{nm} = \chi_{mn} = (-1)^{n+m+1}\,\frac{d}{B} \times \frac{\left[U_{m-1}(x) + (1-\alpha)\,U_{m-2}(x)\right]\,U_{N-n-1}(x)}{U_{N-1}(x) + (1-\alpha)U_{N-2}(x)}\,, \tag{5.12}$$

$$n \geqslant m\,, \qquad n, m = 1, 2, \ldots, N-1\,.$$

In the static case, spatial correlation functions can be found with the aid of formulas (5.8)–(5.12). Essentially, integration in (5.8) can be performed in a range from 0 to ∞, because in supported films, unlike (5.10), all elements of matrix $\hat{M}^{-1}$ remain finite:

$$\left(\hat{M}^{-1}\right)_{nm}(0) = \frac{d}{B}\,(N-m)\,, \tag{5.13}$$

$$n \geqslant m\,, \qquad n, m = 1, 2, \ldots, N-1\,,$$

$$\left(\hat{M}^{-1}\right)_{nm} = \left(\hat{M}^{-1}\right)_{mn}\,.$$

At $q_\perp \to \infty$, matrix elements rapidly decrease (5.11), as in the case of freely suspended films.

Calculated dependences of mean squared fluctuations $\langle|u_n(0)|^2\rangle$ on the layer index in films of different thickness indicate that the effect of the fastened layer spreads deep into the film. The spatial correlation function $\langle u_n(\mathbf{r}_\perp)\,u_m(0)\rangle$ in supported films rapidly decays unlike that in freely suspended ones.

Any real surface exhibits roughness that varies at a characteristic length ζ. Smectics are peculiar in that even a slight modulation of their surface affects deep-lying layers too. The penetration depth, l, can be expressed as $l \sim \zeta^2\sqrt{B/K}$ [1, 2]. Reference [38], describing correlation properties of smectic films fastened to a substrate, takes into consideration both thermal fluctuations and substrate roughness, whose contributions are assumed to be independent. The contribution of substrate roughness to the correlation function can be assessed from the displacement distribution in the smectic film at a given distribution of displacements on the substrate. For this purpose, it is convenient to first solve the Euler–Lagrange equation for displacements inside the film,

$$B\,\frac{\partial^2 u}{\partial z^2} - Kq_\perp^4 u = 0 \tag{5.14}$$

at given surface displacements $u_+(\mathbf{q}_\perp)$ and $u_-(\mathbf{q}_\perp)$, where the plus and minus signs refer to free surface ($z = L/2$) and substrate ($z = -L/2$, L is the film thickness), respectively. The solution for Eqn (5.14) has the form

$$u(\mathbf{q}_\perp, z) = p_+(\mathbf{q}_\perp, z)\,u_+(\mathbf{q}_\perp) + p_-(\mathbf{q}_\perp, z)\,u_-(\mathbf{q}_\perp)\,, \tag{5.15}$$

where

$$p_\pm(\mathbf{q}_\perp, z) = \pm\frac{\sinh\left[\lambda q_\perp^2 (z \pm L/2)\right]}{\sinh(\lambda q_\perp^2 L)}\,, \quad \lambda = \sqrt{\frac{K}{B}}. \tag{5.16}$$

The contribution to the free energy of deformation due to surface displacements is [7, 38]

$$F_{\mathbf{q}_\perp} = \frac{1}{2}\,q_\perp^2\left\{\gamma'_+ u_+^2(\mathbf{q}_\perp) + \gamma'_- u_-^2(\mathbf{q}_\perp) + \frac{\sqrt{BK}}{\sinh(\lambda q_\perp^2 L)} \times \left\{\left[u_+^2(\mathbf{q}_\perp) + u_-^2(\mathbf{q}_\perp)\right]\cosh(\lambda q_\perp^2 L) - 2u_+(\mathbf{q}_\perp)\,u_-(\mathbf{q}_\perp)\right\}\right\}, \tag{5.17}$$

where the coefficients $\gamma'_\pm = \gamma_\pm + K_\pm q_\perp^2$ stand for the surface tensions. Since the displacement distribution is governed by substrate roughness only at the lower film surface, the distribution of free-surface displacements can be found by minimizing the function $F_{\mathbf{q}_\perp}$ with respect to argument $u_+(\mathbf{q}_\perp)$. This permits the expression of free-surface displacements through the displacements on the substrate:

$$u_+(\mathbf{q}_\perp) = s(\mathbf{q}_\perp)\,u_-(\mathbf{q}_\perp)\,, \tag{5.18}$$

where

$$s(\mathbf{q}_\perp) = \frac{1}{v_+\sinh(\lambda q_\perp^2 L) + \cosh(\lambda q_\perp^2 L)}\,, \quad v_\pm = \frac{\gamma'_\pm}{\sqrt{BK}}\,.$$

Formulas (5.15), (5.16), and (5.17) make it possible to obtain an expression for displacements across the entire smectic film if those of the lower boundary layer are given by substrate roughness:

$$u(\mathbf{q}_\perp, z) = y(\mathbf{q}_\perp, z)\,u_-(\mathbf{q}_\perp)\,, \tag{5.19}$$

where

$$y(\mathbf{q}_\perp, z) = p_+(\mathbf{q}_\perp, z)\,s(\mathbf{q}_\perp) + p_-(\mathbf{q}_\perp, z)\,. \tag{5.20}$$

Formula (5.19) allows the spatial correlation function in the smectic film volume to be expressed through the correlation function of substrate roughness $G_-(\mathbf{q}_\perp)$:

$$G(\mathbf{q}_\perp, z, z_1) = \left\langle u(\mathbf{q}_\perp, z)\,u^*(\mathbf{q}_\perp, z_1)\right\rangle = y(\mathbf{q}_\perp, z)\,y(\mathbf{q}_\perp, z_1)\,G_-(\mathbf{q}_\perp)\,. \tag{5.21}$$

For G_-, the fractal correlation function was used [39], which has the following form in the coordinate representation:

$$G_-(\mathbf{r}_\perp) = \left\langle u_-(\mathbf{r}_\perp)\,u_-(0)\right\rangle = \sigma_-^2\exp\left[-\left(\frac{r_\perp}{\zeta}\right)^{2H}\right], \tag{5.22}$$

where σ_- is the characteristic roughness amplitude, ζ is the correlation length in the substrate plane, and H is the parameter characterizing the shape of roughness.

Calculations have demonstrated that the contribution of thermally driven fluctuations increases with increasing distance from the substrate. Their absolute value depends on the elasticity constant B. In usual thermotropic smectics, $B \sim 10^7$ erg cm^{-3} [1]. In this case, the contribution of thermal fluctuations may be comparable to that of roughness. In smectic films with higher values of $B \sim 2.5 \times 10^9$ erg cm^{-3} [38], the contribution of thermal fluctuations becomes negligibly small.

6. X-ray scattering in smectic films

6.1 Scattered radiation intensity

X-ray scattering is an efficient method for the study of static and dynamic properties of smectic films [4, 6–20, 39–50]. In the first Born approximation, the intensity of X-ray scattering by a film is proportional to the electron-density correlation function:

$$I(\mathbf{q}) \sim \left\langle \rho(\mathbf{q})\,\rho(-\mathbf{q})\right\rangle, \tag{6.1}$$

where $\mathbf{q}$ is the scattering vector. Electron density in a smectic film has the form

$$\rho(\mathbf{r}_\perp, z) = \rho_s\sum_{n=1}^{N}\rho_M\left(z - nd - u_n(\mathbf{r}_\perp, t)\right) = \rho_s\sum_{n=1}^{N}\int\rho_M(z_1)\,\delta\left(z_1 - z + nd + u_n(\mathbf{r}_\perp, t)\right)\mathrm{d}z_1, \tag{6.2}$$

where ρ_s is the surface density of molecules in the smectic layer and ρ_M is the linear electron density in the molecule. Passing to the Fourier spectrum in (6.2) leads, for the correlation function (6.1), to

$$\left\langle \rho(\mathbf{q})\,\rho(-\mathbf{q})\right\rangle = \rho_s^2\sum_{n,m=1}^{N}\int\mathrm{d}\mathbf{r}_\perp\exp\left(-\mathrm{i}\mathbf{q}_\perp\mathbf{r}_\perp\right)\int\mathrm{d}z_1\rho_M(z_1) \times\int\mathrm{d}z_2\,\rho_M(z_2)\int\mathrm{d}z'\exp(-\mathrm{i}q_z z') \times\int\mathrm{d}z''\exp(-\mathrm{i}q_z z'')\left\langle\delta\left(z' - z_1 - nd - u_n(\mathbf{r}_\perp)\right) \times\delta\left(z'' - z_2 - nd - u_m(0)\right)\right\rangle, \tag{6.3}$$

where $\mathbf{q} = (\mathbf{q}_\perp, q_z)$. Integration of δ functions yields

$$\langle \rho(\mathbf{q})\, \rho(-\mathbf{q}) \rangle = \rho_s^2 \sum_{n,m=1}^{N} \int \mathrm{d}\mathbf{r}_\perp \exp\left(-\mathrm{i}\mathbf{q}_\perp \mathbf{r}_\perp\right) \times \int \mathrm{d}z_1 \rho_M(z_1) \int \mathrm{d}z_2\, \rho_M(z_2) \times \left\langle \exp\left(-\mathrm{i}q_z(z_1 - z_2 + (n-m)\, d + u_n(\mathbf{r}_\perp) - u_m(0))\right) \right\rangle . \tag{6.4}$$

In the Gaussian approximation over fluctuations of layer displacements, it is easy to calculate the mean value of the exponential function [36]. The result is

$$\langle \rho(\mathbf{q})\, \rho(-\mathbf{q}) \rangle = \rho_s^2 \left|\rho_M(q_z)\right|^2 \sum_{n,m=1}^{N} \exp\left(-\mathrm{i}q_z(n-m)\, d\right) \times \int \exp(-\mathrm{i}\mathbf{q}_\perp \mathbf{r}_\perp) \times \exp\left(-\frac{q_z^2}{2} \left\langle \left(u_n(\mathbf{r}_\perp) - u_m(0)\right)^2 \right\rangle\right) \mathrm{d}\mathbf{r}_\perp . \tag{6.5}$$

With allowance for the spatial homogeneity of layer-displacement fluctuations, integration over the angles between $\mathbf{q}_\perp$ and $\mathbf{r}_\perp$ yields for the correlation function of electron density

$$\langle \rho(\mathbf{q}) \rho(-\mathbf{q}) \rangle = 2\pi \rho_s^2 \left|\rho_M(q_z)\right|^2 \sum_{n,m=1}^{N} \exp(-\mathrm{i}q_z(n-m)d) \times \exp\left(-\frac{q_z^2}{2}\left(\langle u_n^2(0,0)\rangle + \langle u_m^2(0,0)\rangle\right)\right) \times G_{nm}(q_\perp, q_z)\,, \tag{6.6}$$

where

$$G_{nm}(q_z, \mathbf{q}_\perp, t) = \int_0^L r_\perp J_0(q_\perp r_\perp) \times \exp\left(q_z^2 \langle u_n(r_\perp, t)\, u_m(0,0)\rangle\right) \mathrm{d}r_\perp . \tag{6.7}$$

Here, $J_0(x)$ is the zeroth-order Bessel function.

Formula (6.6) describes the angular dependence of the intensity of X-ray radiation scattered by smectic films. An object of experimental studies is normally either specular scattering with $\mathbf{q}_\perp = 0$ or diffuse scattering depending on $\mathbf{q}_\perp$ in the vicinity of the Bragg peak, most often that of the first order ($q_z = 2\pi/d$). Ordered film structure is studied in the former case and inhomogeneity spectra produced by thermal noise and structural defects in the latter. For the purpose of diffuse scattering calculations, it is convenient to subtract unity from the exponent in expression (6.7), because at $L \to \infty$ it does not change the result at $\mathbf{q}_\perp \neq 0$ but guarantees that the integrand decreases at $\mathbf{r}_\perp \to \infty$ [37, 38].

Figure 6 illustrates the effects of various physical factors on the angular dependence of specular X-ray scattering by a freely suspended five-layer film. Figure 6a demonstrates scattering intensity in a finite system of flat layers without regard for the effect of fluctuation displacements and the molecular form factor $|\rho_M(q_z)|^2$ depending on q_z. The figure shows $N-2$ secondary peaks between two neighboring Bragg peaks that are twice as wide as the remaining ones. If squared fluctuations of layer displacements are additionally taken into account, the q_z dependence of X-ray scattering intensity has the form shown in Fig. 6b. Inclusion of spatial correlations between layer displacements and the molecular form factor leads to the distribution of X-ray radiation intensity presented in Figs 6c and 6d [4].

Figure 7 presents the results of measuring the angular dependence of the intensity of specular X-ray reflection from a freely suspended 20-layer film.

6.2 Effect of thermal fluctuations on the shape of Bragg peaks

Let us now analyze effects of thermal layer displacements on the shape of Bragg peaks. This issue was considered at length in theoretical [11, 14, 15, 51] and experimental [52–55] studies of thick smectic slabs. It is convenient to make this analysis in the framework of the continuous model. Then, the last multiplier in formula (6.5) becomes an infinite function of z and can be written as

$$G_{\mathrm{bulk}}(z, \mathbf{r}_\perp) = \exp\left\{-\frac{1}{2}\, q_z^2 \left\langle \left[u(z, \mathbf{r}_\perp) - u(0,0)\right]^2 \right\rangle\right\} . \tag{6.8}$$

The correlation function in the exponent in (6.8) can be computed by expanding it into a three-dimensional Fourier spectrum and using expressions for the Fourier components of displacement fluctuations in the bulk [53]:

$$g(z, \mathbf{r}_\perp) = \left\langle \left[u(z, \mathbf{r}_\perp) - u(0,0)\right]^2 \right\rangle = \frac{k_B T}{4\pi^3 B} \int_0^\infty \mathrm{d}q_z \int \mathrm{d}\mathbf{q}_\perp \frac{1 - \cos(q_z z + \mathbf{q}_\perp \mathbf{r}_\perp)}{q_z^2 + \lambda^2 q_\perp^4} . \tag{6.9}$$

Integration over q_z leads to

$$g(z, \mathbf{r}_\perp) = \frac{k_B T}{8\pi^2 \sqrt{KB}} \int_0^{q_{\max}} \frac{\mathrm{d}q_\perp}{q_\perp} \times \int_0^{2\pi} \mathrm{d}\varphi \left[1 - \exp(-\lambda q_\perp^2 z)\, \cos(q_\perp r_\perp \cos\varphi)\right] . \tag{6.10}$$

Integration over the angle φ gives

$$g(z, \mathbf{r}_\perp) = \frac{k_B T}{4\pi \sqrt{KB}} \int_0^{q_{\max}} \left[1 - \exp(-\lambda q_\perp^2 z)\, J_0(q_\perp r_\perp)\right] \frac{\mathrm{d}q_\perp}{q_\perp} . \tag{6.11}$$

Integration over $q_\perp$ gives the following expression for $G_{\mathrm{bulk}}(z, \mathbf{r}_\perp)$ [51]:

$$G_{\mathrm{bulk}}(z, \mathbf{r}_\perp) \sim \exp(-2\eta C) \left(\frac{4d^2}{r_\perp^2}\right)^\eta \exp\left[-\eta \mathrm{Ei}\left(\frac{r_\perp^2}{4\lambda z}\right)\right] , \tag{6.12}$$

where

$$\mathrm{Ei}(x) = -\int_{-x}^{\infty} \frac{\exp(-t)}{t}\, \mathrm{d}t$$

is the integral exponent,

$$\eta = \frac{q_z^2 k_B T}{8\pi \sqrt{KB}} , \tag{6.13}$$

and $C = 0.5772\ldots$ is Euler's constant.

It follows from formula (6.12) that the correlation function of layer-displacement fluctuations slowly decays in

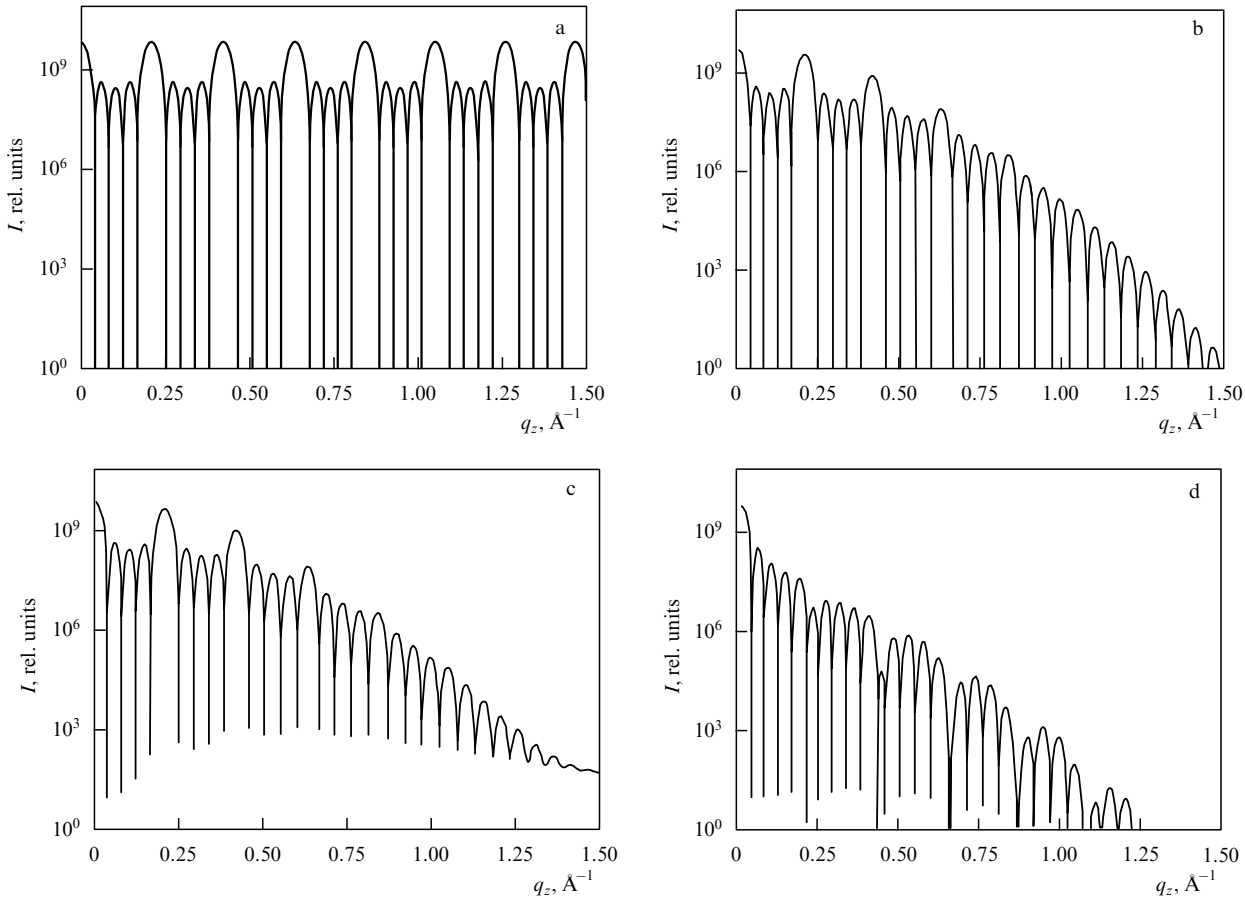

Figure 6. Calculated X-ray specular reflection patterns for a freely suspended five-layer smectic-A film depending on the scattering vector. The calculations were made taking into account (a) finite film thickness alone; (b) finite film thickness and layer-displacement fluctuations; (c) finite film thickness, layer-displacement fluctuations, and correlations between displacements of different layers; and (d) molecular form factor and all aforementioned characteristics [4].

the bulk phase. The decrease is power-like both at $r_\perp = 0$ and $z = 0$:

$$G_{\text{bulk}}(z, r_\perp = 0) \sim \left(\frac{d^2}{\lambda z}\right)^\eta \exp(-\eta C)\,, \tag{6.14}$$

$$G_{\text{bulk}}(z = 0, r_\perp) \sim \left(\frac{4d^2}{r_\perp^2}\right)^\eta \exp(-2\eta C)\,. \tag{6.15}$$

Refs [52–55] report measurements of the profile of the first Bragg peak in the bulk of a smectic-A specimen. Figure 8 shows the results of the measurement of the first Bragg peak in the vicinity of the phase transition to the nematic phase and the results of calculations using formulas (6.5) and (6.12). Evidently, the closer to the nematic phase, the more diffuse is the layered structure of the film, while the elasticity modulus $B \to 0$, and the Bragg peak is less sharp. The values of the parameter η found from the comparison of experimental and theoretical data coincide with those determined from formula (6.6) using known experimental results for elasticity moduli.

Diffuse scattering from a smectic A film is shown in Fig. 9. The solid lines are fits of experimental findings by formula (6.6) taking into consideration instrumental broadening [10]. It should be noted that the correlation functions $\langle u_n(\mathbf{r}_\perp)\, u_m(0)\rangle$ used for the treatment of experimental data were computed in the framework of the continuous model. Specular scattering experiments provide data on the number of film layers, amplitude of layer-displacement fluctuations,

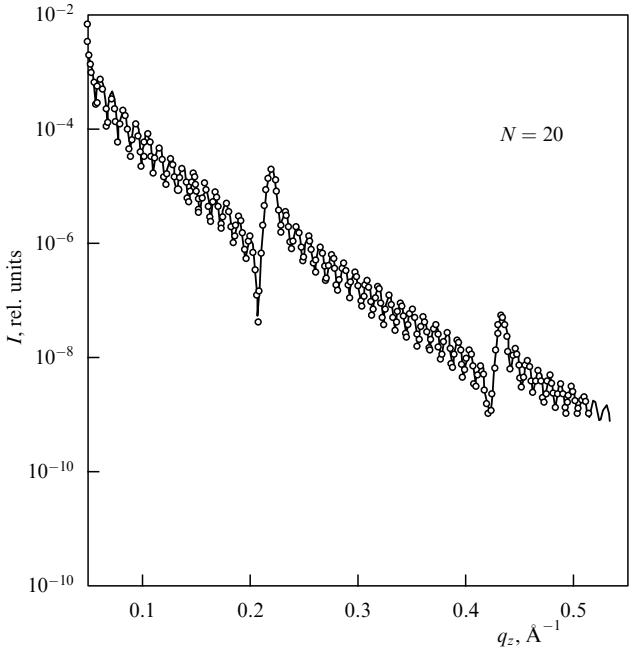

Figure 7. Angular dependence of specular X-ray scattering from a freely suspended 20-layer smectic-A film [10].

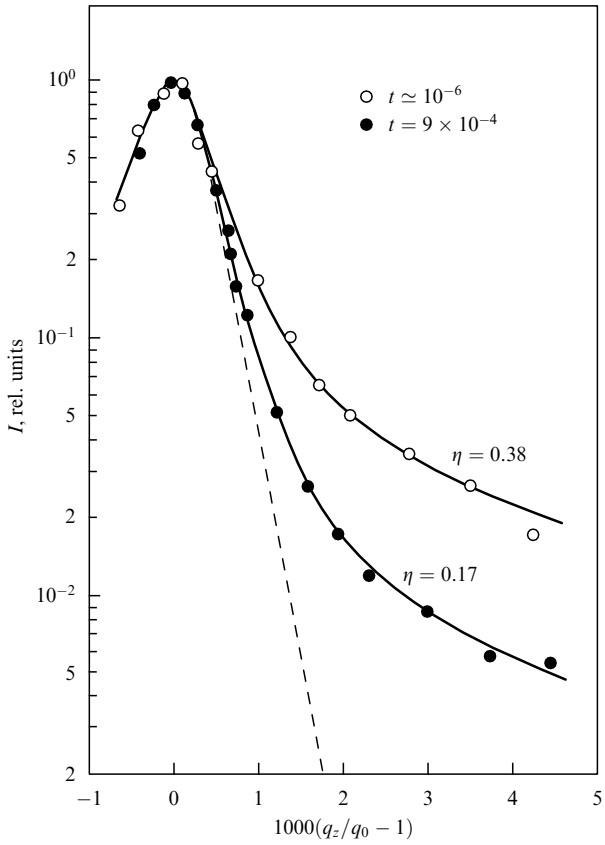

Figure 8. Comparison of experimental and theoretical data at two normalized temperatures $t = |T - T_c|/T_c$ using a single fitting parameter η [55]. The dashed line shows the result of calculations for an ideal infinite smectic.

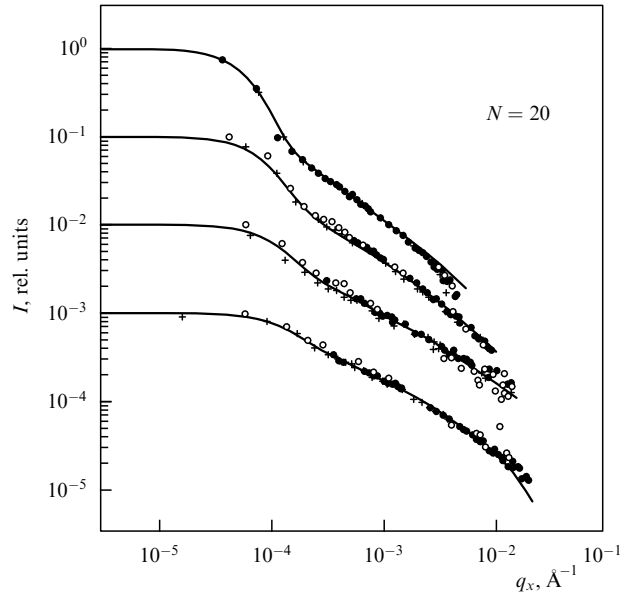

Figure 9. Diffuse X-ray scattering from a freely suspended 20-layer film. The dependence of scattering intensity on the transverse component of the scattering vector q_x is shown as diffuse scans at fixed longitudinal component q_z: 0.216, 0.287, 0.355, and 0.429 Å^{-1} (from top to bottom). The solid lines are theoretical values.

and molecular form factor. Diffuse scattering is interesting in that it bears information about spatial correlations of layer displacements. However, the extraction of information on correlation functions from the results of X-ray scattering experiments is a rather complicated problem.

6.3 Scattering in films on a substrate

In X-ray scattering experiments with the use of films fastened to solid substrates, one of the variables of interest is surface roughness. Hence, smectic films with a small amplitude of thermal layer-displacement fluctuations should be chosen for this purpose. It follows from formula (5.12) that films with an intrinsically large elasticity constant B are especially suitable for experimentation. Figure 10 shows the angular dependence of diffusely scattered light in the vicinity of three Bragg peaks in a smectic-A specimen with $B = 2.5 \times 10^9$ erg cm^{-3}. Assuming that the effect of substrate roughness penetrates deep into the film without decay, the diffuse X-ray scattering data obtained experimentally have been used to restore the fractal roughness correlation function (5.22). This correlation function for

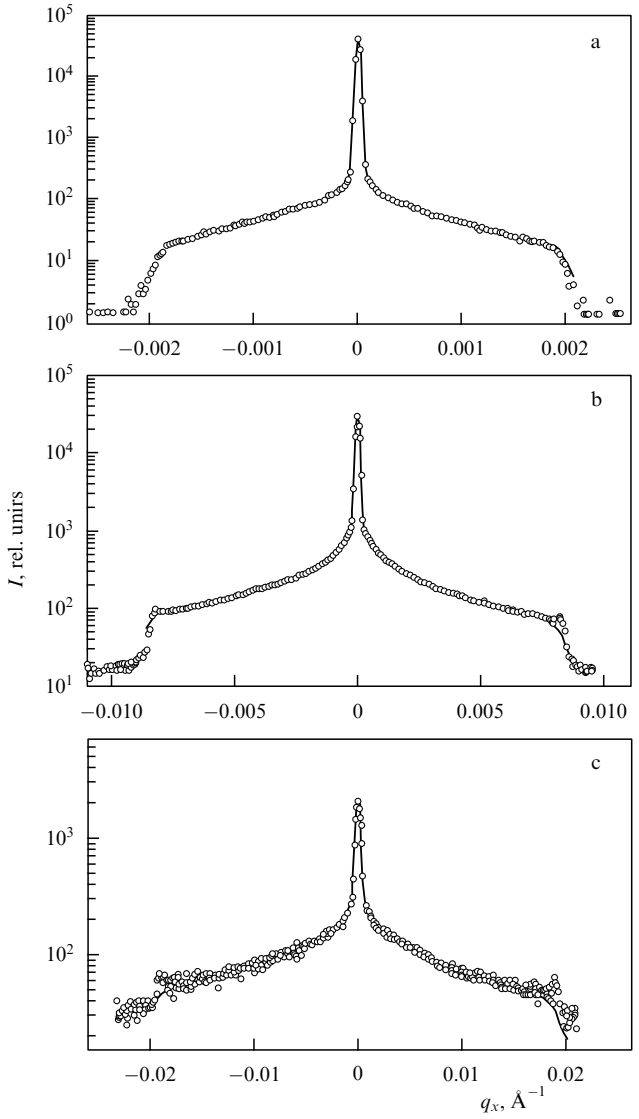

Figure 10. Angular dependence of diffuse X-ray scattering in the vicinity of the first (top), second (center), and third (bottom) Bragg reflections in an M2 smectic sample fastened to a substrate [46].

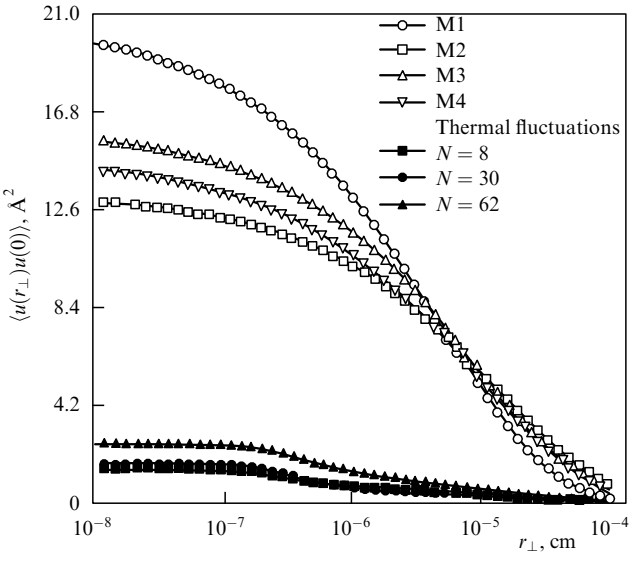

Figure 11. Measured spatial correlation functions $\langle u(r_\perp)\, u(0)\rangle$ for smectic-*C* films of differing thicknesses: M1, 320 Å; M2, 1450 Å; M3, 1500 Å; and M4, 2840 Å. For comparison, the calculated spatial correlation functions of displacement fluctuations for the central layer of 8-layer, 30-layer, and 62-layer polymer films are also plotted [46].

films of different thickness is presented in Fig. 11. For comparison, the same figure also shows the calculated correlation function of thermal displacement fluctuations. Evidently, the B value for a given liquid crystal is sufficiently high to ignore the contribution of thermal fluctuations.

X-ray scattering experiments reported in [47, 56] were carried out on smectic films fastened to a solid substrate. Specifically, Ref. [47] was focused on specular and diffuse scattering from smectic films composed of 22 layers. The experimental data were compared with the results of numerical calculations based on theoretical consideration of solid surface roughness and electron-density distribution across the film. It was demonstrated that experiments yield information about interlayer distances and fluctuations of individual layer displacements.

Interesting measurements of X-ray scattering were made in Ref. [56] using an ultrathin three-layer film fastened to a solid substrate. Two lower layers had a similar composition, whereas the upper monolayer was made of a different material and possessed different optical properties. An X-ray was incident to the surface at nearly grazing angles of 3.5 and 1.5 mrad. The angles were chosen such that total internal reflection from the film/substrate interface occurred at $\theta = 3.5$ mrad. Due to this, the scattered radiation contained information about all three layers. At an angle $\theta = 1.5$ mrad, the radiation was reflected by the lower surface of the outer monolayer, which was therefore the sole layer contributing to scattering. Measurements of scattered radiation intensity depending on q_z and $\mathbf{q}_\perp$ revealed that the scattering patterns were significantly different under these conditions, suggesting the possibility of examining individual monolayers by X-ray probing.

It is worthwhile to note that roughness effects were also studied at the surface of ordinary liquid films [57–60]. Fluctuations of free-surface displacements in such films, like in smectic films, resulted from the collective action of thermal fluctuations (i.e., capillary waves) and surface roughness. The growth of film thickness was accompanied by the crossover from roughness-induced surface fluctuations to thermal fluctuations. Such transition occurred in 50–100 Å thick films which were much thinner than smectic films undergoing a similar transition.

6.4 Dynamic X-ray scattering

Smectic film dynamics is presently studied by correlation spectroscopy for X-ray radiation. This approach has been made possible by the use of synchrotron sources in scattering experiments. The temporal correlation function of scattered X-ray intensities for freely suspended films $\langle I(t)\, I(0)\rangle$ was measured in the immediate vicinity of the first Bragg peak [14, 16, 50]. This correlation function is expressed through the autocorrelation function of Fourier transforms of electron density

$$\langle I(t)\, I(0)\rangle \sim \left|\langle \rho(\mathbf{q}, t)\, \rho(-\mathbf{q}, 0)\rangle\right|^2 . \tag{6.16}$$

The temporal electron density correlation function is defined by formula (6.6) in which a time-dependent function

$$G_{nm}(\mathbf{q}_\perp, q_z, t) = \int_0^L r_\perp J_0(q_\perp r_\perp) \times \exp\left(q_z^2 \langle u_n(r_\perp, t)\, u_m(0,0)\rangle\right) \mathrm{d}r_\perp , \tag{6.17}$$

substitutes for $G_{nm}(\mathbf{q}_\perp, q_z)$.

The problem of finding the temporal correlation function $\langle I(t)\, I(0)\rangle$ therefore reduces to the computation of the temporal layer-displacement correlation function in the coordinate representation $\langle u_n(r_\perp, t)\, u_m(0,0)\rangle$. This function can be expressed through a correlation function in the Fourier representation:

$$\langle u_n(r_\perp, t)\, u_m(0,0)\rangle = \frac{1}{(2\pi)^2}\int_{-\infty}^{\infty} \mathrm{d}\omega \int_{2\pi/L}^{2\pi/a} q_\perp J_0(q_\perp r_\perp) \times \left(u_n(\mathbf{q}_\perp)\, u_m(-\mathbf{q}_\perp)\right)_\omega \exp(-\mathrm{i}\omega t)\, \mathrm{d}q_\perp , \tag{6.18}$$

where the spectral density of displacement fluctuations $(u_n(\mathbf{q}_\perp)\, u_m(-\mathbf{q}_\perp))_\omega$ is given by formula (5.5). Integration over frequencies taking into account expression (5.4) leads to

$$\langle u_n(r_\perp, t)\, u_m(0,0)\rangle = \frac{1}{2\pi}\int_{2\pi/L}^{2\pi/a} q_\perp J_0(q_\perp r_\perp) \times \frac{\omega_-^{(l)} \exp(-\mathrm{i}\omega_+^{(l)} t) - \omega_+^{(l)} \exp(-\mathrm{i}\omega_-^{(l)} t)}{\omega_-^{(l)} - \omega_+^{(l)}} \times \frac{k_\mathrm{B}T}{\lambda^{(l)}(q_\perp)} \frac{u_n^{(l)}(q_\perp)\, u_m^{(l)}(q_\perp)}{\sum_{p=1}^{N}[u_p^{(l)}(q_\perp)]^2}\ \mathrm{d}q_\perp , \tag{6.19}$$

where $\lambda^{(l)}(q_\perp)$ are the eigenvalues of the matrix $\widehat{M}$ (5.7),

$$\lambda^{(l)}(q_\perp) = \frac{2B}{d}\left(1 + x^{(l)}\right) + Kdq_\perp^4 , \tag{6.20}$$

and $u_n^{(l)}(q_\perp)$ are the Fourier components of layer displacements for different modes (3.20). Eigenfrequencies $\omega_\pm^{(l)}$ are defined by formula (3.10). Expression (6.19) at $t = 0$ describes the spatial layer-displacement correlation function.

The contribution of different modes to the correlation function depends in the first place on the amplitude factor $kT/\lambda^{(l)}(q_\perp)$. Note that eigenvalues $\lambda^{(l)}(q_\perp)$ increase with an increasing index of the mode l. Specifically, the first two

modes are easy to estimate as

$$\frac{\lambda^{(1)}(q_\perp)}{\lambda^{(2)}(q_\perp)} \approx \frac{\gamma d N q_\perp^2}{2\pi^2 B} \sim 2 \times 10^{-14} N q_\perp^2 . \qquad (6.21)$$

Thus, the first mode ($l = 1$) makes the major contribution even if N and $q_\perp$ are not very large. Note also that the first mode has the largest relaxation time or the lowest characteristic frequency, which distinguishes the acoustic mode from all the others.

The inset in Fig. 12 shows the experimentally measured temporal correlation function for X-ray scattering intensity for a 95-layer smectic-A film. The solid line shows the same function calculated taking into consideration only the acoustic mode $l = 1$ in expression (6.19).

References [14, 16, 50] report experimental measurements of the relaxation times of the correlation function for X-ray scattering intensities in a variety of smectic-A films differing in the number of layers. It turned out that the measured relaxation times also corresponded to the contribution of the first mode alone to the correlation function:

$$\tau_+^{(1)} = \frac{\eta_3 N d}{2\gamma} . \qquad (6.22)$$

Figure 13 clearly demonstrates the linear dependence of the relaxation times on the film thickness, which is in good agreement with formula (6.22). It should be emphasized that the relaxation regime in the thick films under study is realized practically over the entire measurable range of $q_\perp$ values.

Static specular and diffuse X-ray scattering by freely suspended crystal-B films was experimentally investigated in Ref. [49]. Measurements of the temporal correlation function of X-ray scattering intensities demonstrated that this correlation function closely resembles correlation functions for freely suspended smectic-A films [14, 16, 50]. The X-ray scattering intensities were computed based on theoretical estimates of fluctuations of film-layer displacements. Comparison of numerical calculations and experimental results showed that layer-displacement fluctuations in freely suspended crystal-B films remain unaltered as the film thickness grows, unlike similar fluctuations in smectic-A films, where they increase.

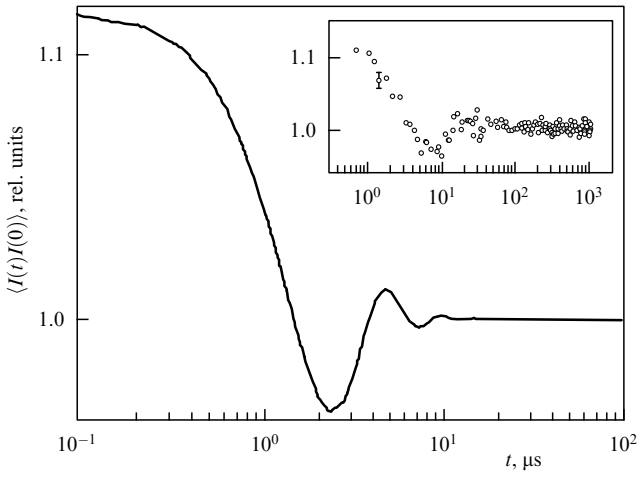

Figure 12. Calculated time dependence of the X-ray scattering intensity autocorrelation function for a freely suspended 100-layer smectic-A film at $q_\perp = 10^3$ cm^{-1} [20]. The inset shows experimental results for a 95-layer film [50].

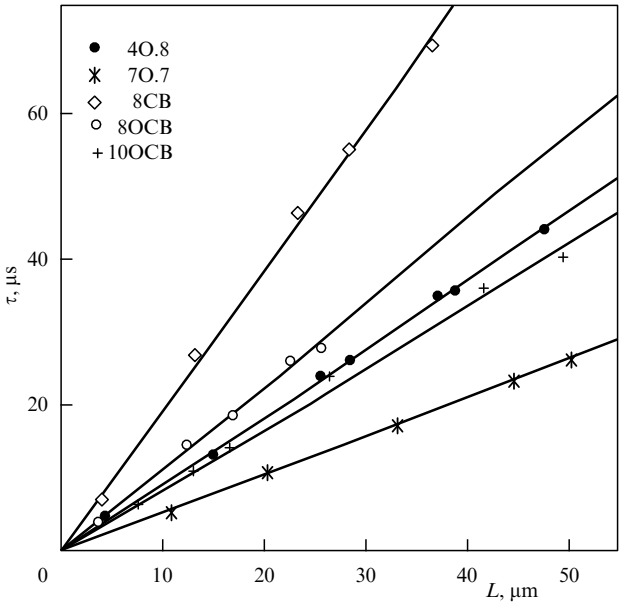

Figure 13. Plots of the decay time $\tau_+^{(1)}$ vs. film thickness for different freely suspended smectics A [16].

7. Light scattering

7.1 Fluctuations of c-director and light scattering in ferroelectric films

The most efficient way to study smectic films is observation of static and dynamic X-ray scattering, because it provides information about film structure and dynamics on interlayer-spacing scales. Another source of data on the film structure is light scattering patterns strongly dependent on director fluctuations. In smectic-A films, director fluctuations $\delta\mathbf{n}$ are almost entirely determined by fluctuations of layer displacements, because $\delta\mathbf{n} = -\nabla_\perp u$ with a high degree of accuracy. This explains why experiments on light scattering in smectics A yield information of the same type as X-ray scattering experiments although on much larger scales, that is, of the order of light wavelength, which is substantially longer than the interlayer distance.

Light scattering techniques are especially efficient in systems where director fluctuations are essentially unrelated to layer displacements. Such systems are exemplified by smectic films in which the director is tilted with respect to the layers. In such films, the projection of the director onto the layer plane is subject to large fluctuations. The amplitude of these fluctuations is determined by Frank moduli and their attenuation by the coefficient of viscosity. For this reason, a study of static and dynamic light scattering in these systems is likely to provide additional information about the structure and dynamics of smectic films. A typical example of these systems is given by freely suspended smectic-C films. The predominant direction of orientation of long molecular axes in smectics C makes an angle θ_T with the normal to a given layer. Projection of the preferred orientation of the molecules onto the layer plane gives rise to a unit vector $\mathbf{c}(\mathbf{r}_\perp)$ called **c-*director*** [1, 2]. This vector on the plane of a

smectic layer is specified by an angle φ with respect to the axis x of the Cartesian coordinate frame in which the axis z coincides with the direction of the normal to the equilibrium smectic film.

Of special interest is an optical study of ferroelectric smectics C^* having a constant dipole moment defined by the relation

$$\mathbf{P}_0(\mathbf{r}_\perp) = P_0\big[\mathbf{c}(\mathbf{r}_\perp) \times \mathbf{e}_z\big]\,. \tag{7.1}$$

Here, $\mathbf{P}_0(\mathbf{r}_\perp)$ is the dipole moment of the unit film surface and P_0 is its absolute value. Spontaneous polarization has two effects. One is that a weak external electric field $E \sim 5$–$10\ \mathrm{V\,cm^{-1}}$ applied to the film plane allows the **c**-director to be oriented in the layer plane. The other is the cessation of short-range interactions in the smectic film, because fluctuations in the orientation generate a surface charge of density $\sigma = -\mathrm{div}\,\mathbf{P}_0$, hence long-range electric forces.

The energy of **c**-director reorientation in the presence of an external electric field has the form [61, 62]

$$F = \int \mathrm{d}\mathbf{r}_\perp \left\{ \frac{1}{2}\,K_\mathrm{s}(\nabla_\perp \mathbf{c})^2 + \frac{1}{2}\,K_\mathrm{b}(\nabla_\perp \times \mathbf{c})^2 - (\mathbf{P}_0\mathbf{E}) + \int \mathrm{d}\mathbf{r}'_\perp \frac{\big(\nabla_\perp \mathbf{P}_0(\mathbf{r}_\perp)\big)\big(\nabla'_\perp \mathbf{P}_0(\mathbf{r}'_\perp)\big)}{2|\,\mathbf{r}_\perp - \mathbf{r}'_\perp|} \right\}. \tag{7.2}$$

Here, the moduli K_s and K_b are related to the Frank bulk moduli as follows:

$$K_\mathrm{s} = LK_{11}\sin^2\theta_T\,, \tag{7.3}$$

$$K_\mathrm{b} = L(K_{22}\sin^2\theta_T\cos^2\theta_T + K_{33}\sin^4\theta_T)\,.$$

Vector $\mathbf{P_0}$ is related to the polarization vector $\mathbf{P}$ by the expression $\mathbf{P_0} = L\mathbf{P}$.

Formula (7.2) is used to compute **c**-director fluctuations. If an external field $\mathbf{E}$ is assumed to lie along the y axis and the equilibrium direction of the **c**-director $\mathbf{c}_0$ to coincide with the x axis, then the disequilibrated **c**-director vector may be represented in the form

$$\mathbf{c}(\mathbf{r}_\perp) = \left(\left(1 - \frac{1}{2}\,(\delta c_y)^2\right), \delta c_y\right).$$

For the free energy in the Gaussian approximation, we obtain

$$F = \frac{1}{2}\int \mathrm{d}\mathbf{r}_\perp \left\{ K_\mathrm{s}\left(\frac{\partial \delta c_y}{\partial y}\right)^2 + K_\mathrm{b}\left(\frac{\partial \delta c_y}{\partial x}\right)^2 - 2P_0E + P_0E(\delta c_y)^2 + P_0^2 \int \mathrm{d}\mathbf{r}'_\perp \frac{\partial \delta c_y}{\partial x}\,\frac{\partial \delta c_{y'}}{\partial x'}\,\frac{1}{|\mathbf{r}_\perp - \mathbf{r}'_\perp|} \right\}. \tag{7.4}$$

Expansion of **c**-director fluctuations into a two-dimensional Fourier spectrum and substitution into free-energy expression (7.4) gives

$$F = \frac{S}{2}\sum_{\mathbf{q}_\perp} \left(K_\mathrm{s}q_y^2 + K_\mathrm{b}q_x^2 + P_0E + 2\pi P_0^2\,\frac{q_x^2}{q_\perp} \right) |c_{\mathbf{q}_\perp}|^2. \tag{7.5}$$

This formula may be used to find director fluctuations [36] in the plane of a ferroelectric smectic C^* [2, 61]:

$$\big\langle |\delta c_{\mathbf{q}_\perp}|^2 \big\rangle = \frac{k_\mathrm{B}T}{S\big(K_\mathrm{s}q_y^2 + K_\mathrm{b}q_x^2 + P_0E + 2\pi P_0^2\,q_x^2/q_\perp\big)}\,. \tag{7.6}$$

Interestingly, there is a possibility to independently observe director fluctuations caused by longitudinal and transverse bends. Indeed, at $q_x = 0$ we obtain the expression for director fluctuations induced by transverse bending

$$\big\langle |\delta c_{\mathbf{q}_\perp}|^2 \big\rangle = \big\langle |\delta c_{q_y}|^2 \big\rangle = \frac{k_\mathrm{B}T}{S(K_\mathrm{s}q_y^2 + P_0E)}\,, \tag{7.7}$$

and at $q_y = 0$ we obtain director fluctuations in the case of longitudinal bending

$$\big\langle |\delta c_{\mathbf{q}_\perp}|^2 \big\rangle = \big\langle |\delta c_{q_x}|^2 \big\rangle = \frac{k_\mathrm{B}T}{S\big(K_\mathrm{b}q_x^2 + P_0E + 2\pi P_0^2\,|q_x|\big)}\,. \tag{7.8}$$

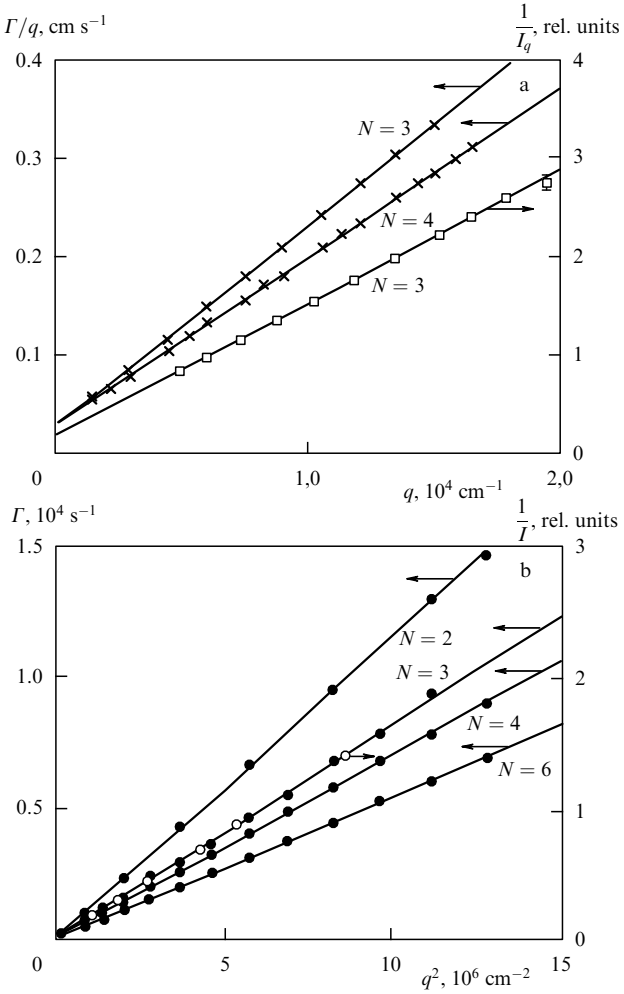

Figure 14. (a) Plots of the decay rate (crosses) and the scattered light intensity (squares) vs. wave number q for the longitudinal bend mode in freely suspended ferroelectric smectic-C films (8O.5*) with different numbers of layers N. The values of $K_\mathrm{b}/\eta_\mathrm{b}$ (in 10^{-5} cm^2 s^{-1} units) as obtained from the slopes of each line to an accuracy of ±2 % are 2.05 ($N = 3$) and 1.7 ($N = 4$). The values of K_b/P_0^2 (in CGS units) obtained from the intercept of the decay curves and the axis of ordinates are $(0.5 \pm 0.02) \times 10^{-2}$ ($N = 3$) and $(4.0 \pm 0.2) \times 10^{-2}$ ($N = 4$). The value of K_b/P_0^2 for ($N = 3$) found from the scattered light intensity equals $(0.8 \pm 0.2) \times 10^{-2}$. (b) Plots of the decay rate (filled circles) and the scattered light intensity (open circles) vs. wave number q for the transverse bend mode in freely suspended ferroelectric smectic-C films (8O.5*) with different numbers of layers N. The values of $K_\mathrm{s}/\eta_\mathrm{s}$ (in 10^{-5} cm^2 s^{-1} units) as obtained from the slopes to an accuracy of ±2 % are 11.7 ($N = 2$) 8.3 ($N = 3$), 7.1 ($N = 4$), and 5.5 ($N = 6$) [61].

The temporal correlation function of these fluctuations has the form

$$\langle \delta c(t)\, \delta c(0)\rangle = \langle |\delta c|^2\rangle \exp(-\Gamma t)\,, \tag{7.9}$$

where

$$\Gamma = \Gamma_{\rm s} = \tau_{\rm s}^{-1} = \frac{K_{\rm s} q_y^2 + P_0 E}{\eta_{\rm s}} \tag{7.10}$$

at $q_x = 0$ and

$$\Gamma = \Gamma_{\rm b} = \tau_{\rm b}^{-1} = \frac{K_{\rm b} q_x^2 + P_0 E + 2\pi P_0^2 |q_x|}{\eta_{\rm b}}$$

at $q_y = 0$. Here, $\eta_{\rm s}$ and $\eta_{\rm b}$ are the viscosity coefficients that describe the relaxation of transverse and longitudinal bends, respectively.

Light scattering intensities and temporal correlation functions for smectic films with various numbers of layers were measured in [61, 62]. Figure 14 presents the decay rates $\Gamma_{\rm s}$ and $\Gamma_{\rm b}$ and the scattered light intensities obtained in one of these works. It appears from formula (7.10) that, for weak external orientation fields ($E \sim 10$ V cm^{-1}), the values of $K_{\rm s}/\eta_{\rm s}$ and $K_{\rm b}/\eta_{\rm b}$ can be obtained from the slopes of temporal correlation functions. Also, it was shown that the decay rate Γ decreases with increasing number of smectic layers. It follows from formulas (7.3) and (7.10) that this effect can be due to the dependence of Frank moduli on film thickness, viscosities, and tilt angles of long molecules in a given layer. This problem was analyzed in [62]. To this effect, scattered light intensities were measured in the presence of two fields: a constant weak electric field $E_{\rm a} = 4$ V cm^{-1} and a rectangular pulsed electric field of amplitude $E_0 = 300$ V cm^{-1} and pulse duration 1.8 ms. Such a design of the experiment permitted the researchers to find the moduli $K_{\rm s}$ and $K_{\rm b}$ and the polarization P_0 at different q_x and q_y. Moreover, measurements of scattered light intensities after elimination of the pulse provided information about the decay rates $\Gamma_{\rm s}$ and $\Gamma_{\rm b}$.

Measurements of scattered light intensities revealed that the Frank moduli exhibit weak dependence on the film thickness, whereas the tilt angle of the director is strongly dependent on the same variable. This dependence is illustrated by Fig. 15, from which it can be seen that the angle θ_T markedly decreases with increasing film thickness and approximates that in the bulk phase. The thickness dependences of both the scattered light intensity and the temporal correlation function indicate that the viscosities $\eta_{\rm s}$ and $\eta_{\rm b}$ increase with film thickness.

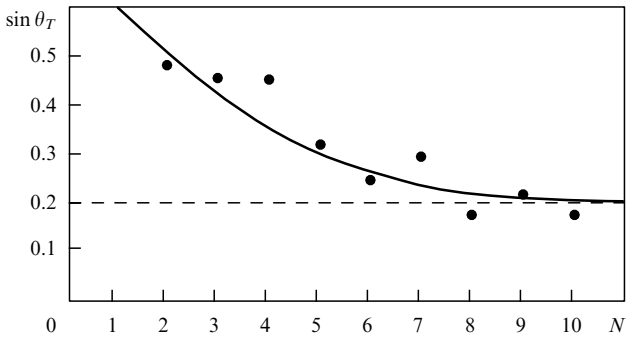

Figure 15. Tilt angle θ_T for a ferroelectric smectic C (DOBAMBC) vs. the number of layers N at $T = 91.5$°C. The dashed line shows the bulk values of θ_T [62].

7.2 Light scattering in smectics *I* and *F*

Smectic films in the I and F phases are interesting objects of research [63 – 66]. In these phases, as in smectic C, the director is tilted with respect to the normal to the layers. There is yet an additional feature. Specifically, the centers of molecular masses within each layer are located at the vertices and in the centers of hexagons. It should be emphasized that phases I and F are characterized by the absence of true long-range order in smectic layers but show correlation between positions of hexagonal elements. The smectic phases F and I are different in that the former has a **c**-director oriented along the normal to any two opposite sides of the hexagons, whereas in the latter the **c**-director is oriented parallel to such sides. A decrease in temperature in these systems leads to the formation of a two-dimensional hexagonal lattice and the transition to phases J and G.

In a description of light scattering from smectic I and smectic-F films, the density of free energy of distortion of the director field is characterized not only by **c**-director orientation but also by the direction of hexagonal elements. It may be assumed that the equilibrium configuration in smectics I and F is specified by an external magnetic field applied along the smectic layers, $H_{\rm a} \sim 1.5 \times 10^3$ G. The free energy of distortion is given by two angles: the angle φ, i.e., the deviation of the **c**-director from the x axis depending on the external field, and the angle θ, which defines rotation of hexagons. The two-dimensional density of the free energy of distortion δF_{2D} has the form [67, 68]

$$\begin{aligned}\delta F_{2D} = {} & \frac{1}{2} K_1^B \left|\frac{\partial\varphi}{\partial x}\right|^2 + \frac{1}{2} K_1^S \left|\frac{\partial\varphi}{\partial y}\right|^2 + \frac{1}{2} K_6^I \left|\frac{\partial\theta}{\partial x}\right|^2 \\ & + \frac{1}{2} K_6^{II} \left|\frac{\partial\theta}{\partial y}\right|^2 - H_6 \cos\left[6(\theta-\varphi)\right] \\ & - H_{12} \cos\left[12(\theta-\varphi)\right], \end{aligned} \tag{7.11}$$

where K_1^B and K_1^S are the elastic moduli related to the distortion of the director field, K_6^I and K_6^{II} are the elastic moduli determined by the distortion of the hexagonal structure in the layers, and H_6 and H_{12} are the moduli associated with the divergence of the **c**-director and hexagon orientations. The light is scattered from fluctuations of the **c**-director, which have the following form in the Gaussian approximation:

$$\langle |\varphi(\mathbf{q}_\perp)|^2\rangle = \frac{k_{\rm B}T}{K_+(\chi)\, q_\perp^2} + \frac{K_-^2(\chi)}{K_1^2(\chi)} \frac{k_{\rm B}T}{H + K_-(\chi)\, q_\perp^2}\,, \tag{7.12}$$

where

$$K_+ = K_1 + K_6\,, \qquad K_- = \frac{K_1 K_6}{K_1 + K_6}\,,$$

$$\mathbf{q}_\perp = q_\perp(\cos\chi,\, \sin\chi, 0)\,,$$

$$K_1(\chi) = K_1^B \cos^2\chi + K_1^S \sin^2\chi\,,$$

$$K_6(\chi) = \begin{cases} K_6^I \cos^2\chi + K_6^{II} \sin^2\chi\,, & \text{Sm-}I\,, \\ K_6^{II} \cos^2\chi + K_6^I \sin^2\chi\,, & \text{Sm-}F, \end{cases}$$

$$H = \begin{cases} 36(H_6 + 4H_{12})\,, & \text{Sm-}I\,, \\ 36(-H_6 + 4H_{12})\,, & \text{Sm-}F. \end{cases}$$

As regards the free energy of distortion in thick films, the variation of the angles θ and φ from layer to layer should be taken into account. In a film of N layers, the wave vector component along the z axis may be assumed to run through a discrete row of values $q_z = n\pi/L, n = 1, 2, \ldots, N$. Then, in the lowest approximation, the three-dimensional density of free energy δF_{3D} can be represented in the form

$$\delta F_{3D} = \delta F_{2D} + \frac{K_1^T}{2}\left(\frac{n\pi}{L}\right)^2 |\varphi(\mathbf{q})|^2 + \frac{K_6^z}{2}\left(\frac{n\pi}{L}\right)^2 |\theta(\mathbf{q})|^2 , \tag{7.13}$$

where $\mathbf{q} = (\mathbf{q}_\perp, n\pi/L)$, and K_1^T and K_6^z are the elastic moduli.

The fluctuating component of the free energy is given by the expression

$$\sum_{\mathbf{q}} \delta F_{3D} = S \sum_{n=1}^{N} \int \delta F_{3D}\, \mathrm{d}\mathbf{q}_\perp ,$$

where S is the film area. Expression (7.13) can contain other terms permissible by symmetry considerations, but they make no appreciable contribution in light scattering experiments on smectic films [66]. Ref. [66] provides experimental data on light scattering from a freely suspended 8OSI crystal film in smectic I and C phases. The authors worked with both thick film specimens ($L = 3$ μm) and thin films containing a few layers. For the case of normal incidence, the scattered light intensity in thick films was described by the expression

$$I_{\mathrm{sc}} = I_0 \sin^2\theta_T \sin^2(\theta_T + \theta_{\mathrm{s}}) \left[\frac{1}{Aq_x^2} + \frac{1}{C + Bq_x^2}\right], \tag{7.14}$$

where θ_T is the equilibrium tilt of the director relative the normal to the layers, θ_{s} is the angle between the scattered ray direction and the normal to the layers, $\mathbf{q}_\perp = (q_x, 0)$, $q_x = k \sin\theta_{\mathrm{s}}$, and k is the wave number of the incident wave.

Figure 16 presents scattered light intensity in thick films of smectics C and I as a function of temperature and wave number component q_x. The experimental data are fairly well described by expression (7.14) and can be used to find the temperature dependence of the effective orientational elasticity modulus. The noticeable curvature of the dependence of the scattering intensity on q_x is largely attributable to the factor $\sin^2(\theta_T + \theta_{\mathrm{s}})$ in expression (7.14). It has been shown that the effective orientational elasticity modulus in the smectic I phase is one or two orders of magnitude that in phase C. Similar measurements in thin films composed of two and four smectic layers agree equally well with theoretical predictions.

Measurements of scattered light intensity in two geometries, i.e., when the scattering vector component was parallel to the external magnetic field and when it was normal to the field, were used to find longitudinal and transverse bend moduli. Temperature dependences of these moduli for a three-layer (8OSI) film are presented in Fig. 17. Note that the description of these dependences needs to take into account only the acoustic mode in which both the **c**-director and the hexagonal structure undergo in-phase deviations from the equilibrium direction. But in the case under consideration, measurements of the half-width of the central component of the scattering spectrum were employed to determine the effective viscosity. Note that the $I-C$ phase-transition temperature in the thin film was much higher than in the bulk.

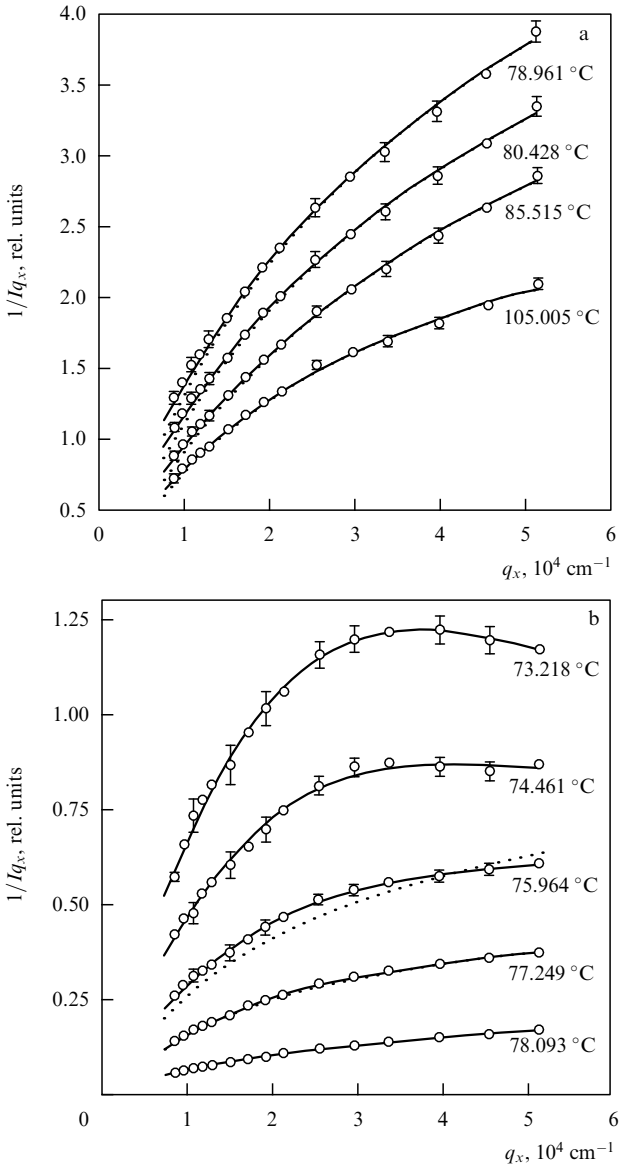

Figure 16. Angular dependence of scattered light intensity on the acoustic mode in a 3 μm 8OSI smectic film in longitudinal bending geometry. The lines are variants of the adjusting of experimental data by formula (7.14): (a) phase C and (b) phase I [66].

References [69] reports a study of light scattering from freely suspended thin films in smectic-C^* and hexatic-I^* phases. Formulas used to describe light scattering in the hexatic-I^* phase were analogous to those cited above for smectic C^*. The authors measured the elastic moduli and the relaxation times of longitudinal and transverse bend distortions. It was found that the moduli of elasticity increased by one or two orders of magnitude upon the C^*-I^* phase transition. Also, a transition to the I^* phase resulted in a larger longitudinal bend modulus K_{b} as compared to the transverse bend modulus K_{s}.

Measurements of temporal correlation functions of scattered-light intensities in the hexatic I^* phase revealed that their decay was a consequence of two relaxation processes. Measurements at different scattering angles showed that one of these processes was linked to the acoustic mode, while the other was associated with the optical mode in

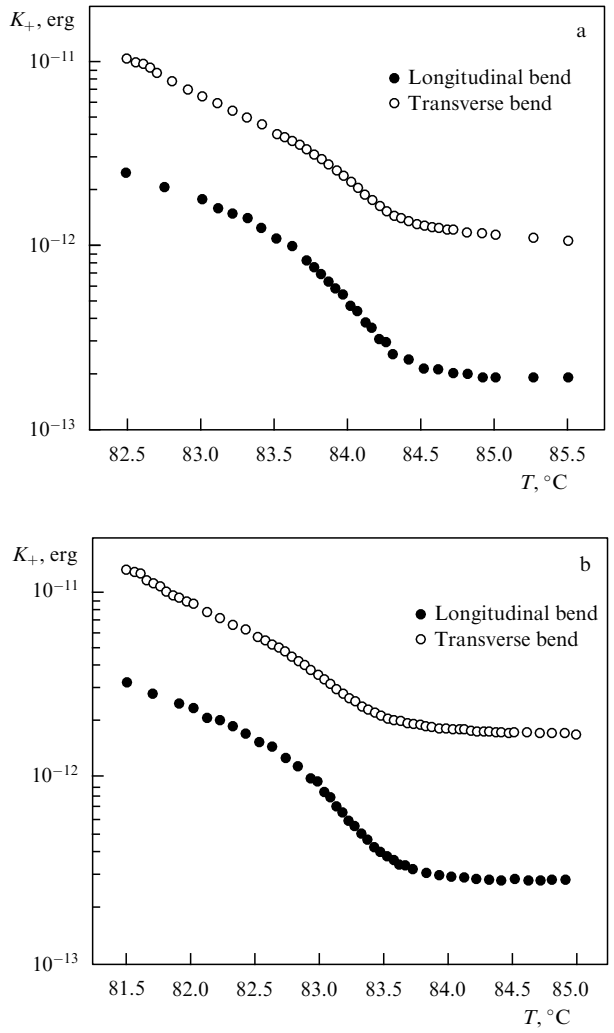

Figure 17. Temperature dependence of the moduli K_+^B and K_+^S determining the longitudinal and transverse bends of (a) two-layer and (b) three-layer 8OSI smectic films in the vicinity of the $C-I$ transition point at T_L [66].

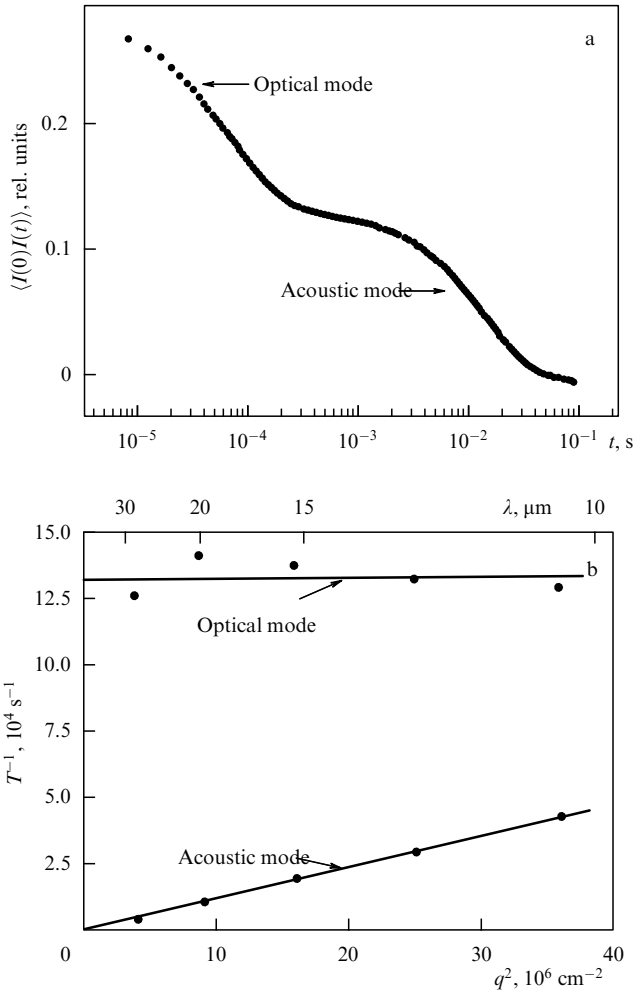

Figure 18. (a) Dynamic correlation function for a five-layer film in the hexatic I^* phase 1.2 K below the point of transition to the smectic-C^* phase. (b) Wave-vector dependence of the relaxation rates of the optical and acoustic modes [69].

which fluctuations of the **c**-director and the whole structure occurred in the antiphase. The results of these measurements are presented in Fig. 18.

An interesting result was obtained in Refs [70, 71]. It was shown by means of an optical technique that the polarization vector in a ferroelectric smectic-C^* liquid-crystal film could be oriented either normal or parallel to the **c**-director. This effect was absent in very thin films and emerged as their thickness increased. In particular, the polarization vector in a 20-layer film of DOBAMBC smectic liquid crystal was perpendicular to the **c**-director below 12 °C and parallel to it at higher temperatures. The authors attributed this finding to smectic-C^* – smectic-A phase transition that occurred in this temperature range starting from inner layers. This means that the director in these layers was oriented normally to them. Conversely, the director orientations in outer layers were independent of one another. In this situation, the C-like configuration in an external field was energetically more advantageous than the S-like configuration. Such a transformation is shown in Fig. 19. The changing orientation of the director across the film thickness was responsible for flexoelectric polarization [1] that had the same direction in the vicinity of the

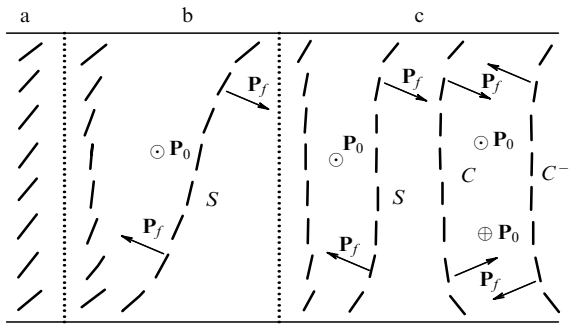

Figure 19. Molecular orientation in a freely suspended thick smectic film (a) below and (b) above the bulk $C-A$ phase transition temperature; (c) Formation of S-, C-, and C-like configurations far above the transition point. $\mathbf{P}_0$ and $\mathbf{P}_f$ are the ferroelectric and flexoelectric polarization vectors, respectively [70, 71].

transition point to smectic phase A as the **c**-director. With the approach to the transition point, the ferroelectric polarization became weaker than the flexoelectric one, which caused the polarization vector to rotate.

8. Conclusion

We have considered various characteristics of smectic films. A remarkable property of these films is their liquid-like and crystal-like behavior. As a result, they exhibit both acoustic and optical vibrations of individual layers and show Bragg peaks in X-ray scattering spectra, Rayleigh waves at the surface, and spontaneous polarization in ferroelectric films. At the same time, the dynamic properties and the structure of these films are strongly influenced by surface tension, shear viscosity, external fields, etc.

Unlike other types of liquid-crystal films, smectic films have a rather simple layered structure, allowing a consistent theoretical description of their static and dynamic properties. In this context, smectic films provide a most convenient model for the investigation of physical characteristics of two-dimensional systems. Experimental techniques and theoretical approaches being developed for this purpose are expected to promote a deeper insight into the nature of both liquid and solid films.

At the same time, many problems associated with the use of smectic films as convenient research systems remain unresolved. These are investigations into dynamic properties of multilayer films, extraction of information about film characteristics (first and foremost, correlation properties) from the data on specular and diffuse X-ray scattering, and the use of dynamic X-ray scattering for the study of dynamic properties of a broader class of smectic films. Further development of the theory of phase transitions in thin films is needed, as is a more consistent analysis of numerous experimental findings pertinent to phase transitions. Such studies would bring in new knowledge of film structure and dynamic properties.

This work was supported by the Russian Foundation for Basic Research (grant Nos. 03-02-16173 and 02-02-16577).

References

1. De Gennes P-G *The Physics of Liquid Crystals* (Oxford: Clarendon Press, 1974) [Translated into Russian (Moscow: Mir, 1977)]
2. de Gennes P G, Prost J *The Physics of Liquid Crystals* 2nd ed. (Oxford: Clarendon Press, 1993)
3. Landau L D, Lifshitz E M *Teoriya Uprugosti* (Theory of Elasticity) (Moscow: Nauka, 1987) [Translated into English (Oxford: Pergamon Press, 1986)]
4. Holyst R *Phys. Rev. A* **44** 3692 (1991)
5. Martin P C, Parodi O, Pershan P S *Phys. Rev. A* **6** 2401 (1972)
6. Chen H-Y, Jasnow D *Phys. Rev. E* **57** 5639 (1998)
7. Poniewierski A, Holyst R *Phys. Rev. B* **47** 9840 (1993)
8. Shalaginov A N, Romanov V P *Phys. Rev. E* **48** 1073 (1993)
9. Shindler J D et al. *Phys. Rev. Lett.* **74** 722 (1995)
10. Mol E A L et al. *Phys. Rev. E* **54** 536 (1996)
11. Chen H-Y, Jasnow D *Phys. Rev. E* **61** 493 (2000)
12. Shalaginov A N, Sullivan D E *Phys. Rev. E* **62** 699 (2000)
13. Holyst R *Phys. Rev. A* **42** 7511 (1990)
14. Poniewierski A et al. *Phys. Rev. E* **58** 2027 (1998)
15. Poniewierski A et al. *Phys. Rev. E* **59** 3048 (1999)
16. Price A C et al. *Phys. Rev. Lett.* **82** 755 (1999)
17. Mirantsev L V *Fiz. Tverd. Tela* **41** 1882 (1999) [*Phys. Solid State* **41** 1729 (1999)]
18. Mirantsev L V *Phys. Rev. E* **62** 647 (2000)
19. Romanov V P, Ul'yanov S V *Phys. Rev. E* **63** 031706 (2001)
20. Romanov V P, Ul'yanov S V *Phys. Rev. E* **65** 021706 (2002)
21. Brillouin L, Parodi M *Wave Propagation in Periodic Structures* (New York: Dover Publ., 1953) [Translated into Russian (Moscow: IL, 1959)]
22. Abramowitz M, Stegun I A (Eds) *Handbook of Mathematical Functions with Formulas, Graphs, and Mathematical Tables* (New York: Dover Publ., 1965) [Translated into Russian (Moscow: Nauka, 1979)]
23. Miyano K *Phys. Rev. A* **26** 1820 (1982)
24. Stoebe T, Mach P, Huang C C *Phys. Rev. E* **49** R3587 (1994)
25. Stoebe T et al. *Phys. Rev. E* **53** 1662 (1996)
26. Romanov V P, Ul'yanov S V *Phys. Rev. E* **66** 061701 (2002)
27. Orsay Group on Liquid Crystals. *J. Phys. Colloq.* (Paris) **36** (Suppl. C1) C1-305 (1975)
28. Landau L D, Lifshitz E M *Gidrodinamika* (Fluid Mechanics) (Moscow: Nauka, 1986) [Translated into English (Oxford: Pergamon Press, 1987)]
29. Fedorov D O, Romanov V P, Ul'yanov S V *Phys. Rev. E* **62** 681 (2000)
30. Eĭdel'man E D *Poverkhnost'*: *Fiz. Khim. Mekh.* (3) 26 (1995)
31. Dorshow R B, Turkevich L A *Phys. Rev. Lett.* **70** 2439 (1993)
32. Cao B H, Kim M W, Cummins H Z *J. Chem. Phys.* **102** 9375 (1995)
33. Huang Q R, Wang C H *J. Chem. Phys.* **105** 6546 (1996)
34. Monroy F, Langevin D *Phys. Rev. Lett.* **81** 3167 (1998)
35. Huang Q R, Wang C H, Deng N J *J. Chem. Phys.* **108** 3827 (1998)
36. Landau L D, Lifshitz E M *Statisticheskaya Fizika* Ch. 1 (Statistical Physics. Pt. 1) (Moscow: Nauka, 1976) [Translated into English (Oxford: Pergamon Press, 1980)]
37. de Boer D K G *Phys. Rev. E* **59** 1880 (1999)
38. Sinha S K et al. *Phys. Rev. B* **38** 2297 (1988)
39. de Jeu W H, Ostrovskii B I, Shalaginov A N *Rev. Mod. Phys.* **75** 181 (2003)
40. Tweet D J et al. *Phys. Rev. Lett.* **65** 2157 (1990)
41. Holyst R, Tweet D J, Sorensen L B *Phys. Rev. Lett.* **65** 2153 (1990)
42. Pieranski P et al. *Physica A* **194** 364 (1993)
43. Mol E A L et al. *Phys. Rev. Lett.* **79** 3439 (1997)
44. Geer R E et al. *Phys. Rev. Lett.* **71** 1391 (1993)
45. Geer R E, Shashidhar R *Phys. Rev. E* **51** R8 (1995)
46. Geer R E et al. *Phys. Rev. E* **52** 671 (1995)
47. de Boer D K G et al. *Physica B* **248** 274 (1998)
48. Salditt T et al. *Phys. Rev. E* **60** 7285 (1999)
49. Fera A et al. *Phys. Rev. E* **63** 020601(R) (2001)
50. Fera A et al. *Phys. Rev. Lett.* **85** 2316 (2000)
51. Caille A *CR Acad. Sci. B* **274** 891 (1972)
52. Als-Nielsen J et al. *Phys. Rev. Lett.* **39** 1668 (1977)
53. Als-Nielsen J et al. *Phys. Rev. B* **22** 312 (1980)
54. Safinya C R et al. *Phys. Rev. Lett.* **57** 2718 (1986)
55. Als-Nielsen J et al., in *Ordering in Strongly Fluctuating Condensed Matter Systems* (NATO Adv. Study Institute Series, Ser. B, Vol. 50, Ed. T Riste) (New York: Plenum Press, 1980) p. 57
56. Dupres V et al. *Phys. Rev. E* **66** 012701 (2002)
57. Andelman D, Joanny J-F, Robbins M O *Europhys. Lett.* **7** 731 (1988)
58. Robbins M O, Andelman D, Joanny J-F *Phys. Rev. A* **43** 4344 (1991)
59. Tidswell I M et al. *Phys. Rev. Lett.* **66** 2108 (1991)
60. Pershan P S *J. Phys.: Condens. Matter* **6** A37 (1994)
61. Young C Y et al. *Phys. Rev. Lett.* **40** 773 (1978)
62. Rosenblatt C et al. *Phys. Rev. Lett.* **42** 1220 (1979)
63. Brock J D et al. *Phys. Rev. Lett.* **57** 98 (1986)
64. Brock J D, Noh D Y, McClain B R *Z. Phys. B: Cond. Mat.* **74** 197 (1989)
65. Cheng M et al. *Phys. Rev. Lett.* **59** 1112 (1987)
66. Sprunt S, Spector M S, Litster J D *Phys. Rev. A* **45** 7355 (1992)
67. Nelson D R, Halperin B I *Phys. Rev. B* **21** 5312 (1980)
68. Bruinsma R, Nelson D R *Phys. Rev. B* **23** 402 (1981)
69. Dierker S B, Pindak R *Phys. Rev. Lett.* **59** 1002 (1987)
70. Andreeva P O et al. *Phys. Rev. E* **59** 4143 (1999)
71. Andreeva P O et al. *Zh. Eksp. Teor. Fiz.* **116** 1329 (1999) [*JETP* **89** 713 (1999)]